Title
Earthquake spatial distribution: the correlation dimension

Journal
Geophysical Journal International, 168(3)

ISSN
0956-540X

Author
Kagan, Yan Y

Publication Date
2007-03-01

PostScript file created: May 10, 2007; time 832 minutes

EARTHQUAKE SPATIAL DISTRIBUTION: THE CORRELATION DIMENSION

Yan Y. Kagan[1]

[1] Department of Earth and Space Sciences, University of California, Los Angeles, California, USA

Abstract. We review methods for determining the fractal dimensions of earthquake epicenters and hypocenters, paying special attention to the problem of errors, biases and systematic effects. Among effects considered are earthquake location errors, boundary effects, inhomogeneity of depth distribution, and temporal dependence. In particular, the correlation dimension of earthquake spatial distribution is discussed, techniques for its evaluation presented, and results for several earthquake catalogs are analyzed. We show that practically any value for the correlation dimension can be obtained if many errors and inhomogeneities in observational data as well as deficiencies in data processing are not properly considered. It is likely that such technical difficulties are intensified when one attempts to evaluate multifractal measures of dimension. Taking into account possible errors and biases, we conclude that the fractal dimension for shallow seismicity asymptotically approaches 2.20 ± 0.05 for a catalog time span of decades and perhaps centuries. The value of the correlation dimension declines to 1.8-1.9 for intermediate events (depth interval 71-280 km) and to 1.5-1.6 for deeper ones. For plate tectonic deformation on the time scale of millions of years, it is possible that the correlation dimension for shallow earthquakes may increase to 2.6–2.7.

INDEX TERMS: 7215 Seismology

KEYWORDS: Earthquake location, Fractals, Geostatistics, Seismicity, Statistical methods, Synthetic-earthquake catalogues

1. Introduction

This paper continues our research into spatial patterns of earthquake occurrence (Kagan & Knopoff 1978, 1980; Kagan 1981a;b; Kagan 1991a). In the last 5-10 years many papers (see below) have been published which analyzed both theoretical and phenomenological aspects of the scale-invariant spatial features of earthquakes. Various values for scaling exponents have been proposed. However, it is not clear whether such diversity is due to real physical reasons or is caused by data deficiencies and failure to consider the properties of earthquake process.

In this paper we analyze the statistical distributions of earthquake epicenters and hypocenters. Since this distribution exhibits scale-invariant properties, it is often called a fractal spatial distribution (Kagan & Knopoff 1978, 1980; Ogata & Katsura 1991; Kagan 1991a; Vere-Jones 1999; Harte 1998, 2001; Bak *et al.* 2002) and is characterized by its fractal and, in particular, correlation dimension, δ. Several sources of random and systematic errors as well as biases in the dimension determination need to be considered first.

As a major tool in this study, we analyze a distribution of distances between any event pairs in several earthquake catalogs. Thus, we study the correlation dimension of earthquake spatial patterns. Studying distances has a certain advantage compared to the widely used box-counting methods for studying fractal patterns. For example, southern California seismicity exhibits clear alignment along the plate boundaries and the San Andreas fault system. It is possible, therefore, that cells oriented along the fault would yield a different result compared to boxes selected along latitude/longitude lines. In addition, the initial grid location and the size of the smallest and largest cells can influence the box-counting algorithm (Molchan & Kronrod 2005).

The distances between events do not depend, as boxes do, on the system coordinates and the grid selection. Moreover, distances can be defined on a surface of a 2-D (two-dimensional) sphere. Box-counting on a spherical surface, when analysis is extended over large spherical regions, cannot be used without unknown modifications at present. This is perhaps one reason why box-counting techniques have been employed in relatively limited seismic regions like California (Geilikman *et al.* 1990; Bak *et al.* 2002; Molchan & Kronrod 2005).

As we will see, investigating local catalogs presents serious problems connected with boundary effects and the high spatial inhomogeneity of the location accuracy and magnitude threshold. These drawbacks are largely due to the spatial boundaries of the catalogs, and are especially strong for networks situated on island chains like Japan and New Zealand where station distribution is almost one-dimensional. Therefore, we should compare results for local or regional catalogs with studies of global earthquake catalogs in which the above problems are significantly alleviated.

For example, Harte and Vere-Jones (1999) paired up the events listed in the PDE and New Zealand catalogs and studied the difference in the tabulated solutions. They found that earthquake epicenters in some regions are systematically displaced in one catalog relative to another, and earthquake depths are often also systematically different. This effect is a natural consequence of different station distribution in these catalogs, as well as different interpretation methods. However, for global catalogs one should expect less variation in location bias, and since in this work we are not interested in real earthquake locations but in distances between catalog solutions, global catalogs may have certain advantages compared to local ones.

In particular, we are interested here primarily in the *hypocentral* fractal pattern, since this pattern characterizes physical properties of the earthquake rupture process.

However, in many earthquake catalogs, unreliable source depth information forces one to study epicentral distribution. Moreover, seismicity is usually concentrated in the upper crust, corresponding to a narrow layer of 15-20 km thickness. For distances exceeding that width, epicentral and hypocentral moments converge (Section 5). Therefore, we consider the interrelationship between these two distributions and show how the epicentral fractal pattern can be used to infer the value of the hypocentral correlation dimension, especially for large distances.

For distances comparable to the seismogenic depth interval, the epicentral distribution may be strongly influenced by projection effects which increase the estimate of the correlation dimension for a set of epicenters. We calculate appropriate corrections so that the biases can be more accurately estimated. Similarly, the hypocentral moment function changes significantly when calculated for a seismogenic layer at distances comparable to or exceeding its thickness.

In most studies of earthquake spatial distribution, location and other errors have not been properly considered. This oversight might explain the high values of fractal dimensions often reported and their great variability, findings which do not reflect the physical and geometrical properties of the earthquake fracture but rather indicate location and projection errors peculiar to the catalogs studied.

The notable feature of the present investigation is its emphasis on analysis of the errors and systematic effects in studying the correlation dimension. As we show, these effects are often so large that they may render the results of any statistical analysis irrelevant, if these influences are not noted.

In Fig. 1 we show epicenters in the catalog compiled by Hauksson & Shearer (2005) (see Section 3 below) for the period 1984-2002. The accuracy of the hypocenter location is very high; in many cases the errors do not exceed 0.1 km. For the faults that are vertical or close to vertical, such as the 1992 Landers (coordinates 34.20° N, 116.44° W – see Kagan *et al.* 2006) or the 1999 Hector Mine (34.59° N, 116.27° W), earthquakes, the epicenters delineate the major faults as well as subsidiary features. However, for the 1994 Northridge earthquake (34.21° N, 118.54° W), epicenters form a cloud. This happens because the rupture plane of the earthquake was far from vertical (Thio & Kanamori 1996).

We can compare Fig. 1 with the epicenter maps for the local catalog for southern California for 1800-2005 (see Kagan *et al.* 2006). This catalog combines historical and instrumental earthquake catalogs. Several features can be seen in that catalog: although most aftershocks of the 1857 Fort Tejon earthquake are likely to be missing, and the location accuracy is low for historic earthquakes, the spatial distribution is more uniform along the San Andreas fault than similar distributions are for the catalogs of a more limited time span.

The earthquakes in Fig. 1 show strong concentration in a few clusters, often connected to the aftershock sequences of strong events. This narrow clustering, as we will see, leads to a decrease in the correlation dimension of earthquake distribution. On the other hand, the broad earthquake distribution such as Fig. 1 in Kagan *et al.* (2006) produces a larger value of that dimension.

Describing scale-invariant point patterns, like that shown in Fig. 1, presents serious methodological and theoretical problems, since the mathematical framework for analysis is not yet completed. The first approach is to treat this pattern as a stochastic point process (Vere-Jones 1999; Daley & Vere-Jones 2003). For such a process the covariance measure C_2 can be defined by

$$C_2(y-x) \;=\; m\,[\,m_1(y|x) - m\,]\,, \qquad (1)$$

where m is a point mean density, and the conditional first moment measure or the Palm intensity $m_1(y|x)$ is a function of distance $y-x$ (Kagan & Vere-Jones 1996). Moment m_1 is proportional to the number of event pairs at various distance intervals measured for each point. In the earthquake applications, $m_1(y|x) >> m$ for $y-x$ small, and probably impossible to determine from a finite data set, whether the power decay relates to $m_1(y|x)$ directly, or to the difference $m_1(y|x) - m$. For fractal distributions the moment m_1 has a power-law dependence on distance R

$$m_1(R) \;\propto\; R^{\delta-1}\,. \qquad (2)$$

Another approach is to use total counts of point pairs in the analysis as they depend on their distance. This is usual treatment of fractal point patterns whether they are encountered in *phase space* of strange attractors (see for example, Nerenberg & Essex 1990 or Harte 2001) or in *real space* of earthquake spatial distribution. In this work, depending on dimensionality D of the space considered, we study the total number of earthquake pairs at distance R

$$N_D(R) \;\propto\; R^{\delta}\,. \qquad (3)$$

Then the simplest estimate of $\hat{\delta}$ is a straight line in a log-log plot N_D versus R, or

$$\hat{\delta} \;=\; \frac{\partial\,[\log N_D(R)]}{\partial\,(\log R)}\,. \qquad (4)$$

Because of different mathematical tools used in the analysis of point patterns, the terminology is not yet stabilized. This is the reason that in various papers (including ours) different terms (like statistical moments or pair numbers, see Eqs. 2 and 3) sometimes are employed to describe the earthquake spatial patterns.

2. Simulating point spatial patterns

Simulating spatial distributions is often necessary in testing formulas to estimate various dimensions of point patterns and different biases caused by location errors and other defects in earthquake data (see Section 4 below).

The non-fractal point distribution can be simulated by placing points randomly in a region of a 2-D plane or 3-D (three-dimensional) volume. The resulting point pattern is a spatial Poisson process. Ripley (1988) and Stoyan & Stoyan (1994) discuss these simulations in more detail.

To simulate random points in a window in a sphere with longitude limits x_1 and x_2 and latitude limits y_1 and y_2, we use the following formula

$$\begin{aligned} x \;&=\; x_1 + Z_1 \times (x_2 - x_1), \quad \text{and} \\ y \;&=\; \arcsin[Z_2 \times (\sin(y_2) - \sin(y_1)) + \sin(y_1)]\,, \end{aligned} \qquad (5)$$

where Z_i are uniformly distributed random numbers in a range $(0,1]$.

To create a point pair for a fractal point pattern, we use Lévy flight pattern (Mandelbrot 1983). We put one point at the center and use the truncated Pareto distribution to simulate the position of a second. The probability density function for the distance r is

$$\phi(r) \;=\; \frac{r_{\max}^{\delta}\, r_{\min}^{\delta}}{r_{\max}^{\delta} - r_{\min}^{\delta}}\,\delta\, r^{\,-1-\delta} \quad \text{for} \quad r_{\min} \le r \le r_{\max}\,, \qquad (6)$$

and the distribution function

$$\Phi(r) \;=\; \frac{(r_{\min}/r)^{\delta} - (r_{\min}/r_{\max})^{\delta}}{1 - (r_{\min}/r_{\max})^{\delta}} \quad \text{for} \quad r_{\min} \le r \le r_{\max}\,, \qquad (7)$$

where $r_{\min}$ and $r_{\max}$ are the minimum and maximum distances, and δ is the dimension of the pattern.

For the truncated Pareto distribution, we simulate distances as

$$r = r_{\min} \left\{ Z \left[1 - (r_{\max}/r_{\min})^{-\delta} \right] + (r_{\max}/r_{\min})^{-\delta} \right\}^{-1/\delta} . \quad (8)$$

where Z is the same as in (5). The random point is then obtained by simulating a normalized random 3-D vector with Marsaglia's (1972) algorithm (see also http://mathworld.wolfram.com/SpherePointPicking.html) and putting a point along the vector at the distance r.

The simulation methods described above have two disadvantages. The points can be too orderly (e.g., the pattern of random points on a 2-D plane or spherical surface as in Eq. 5). Or with the other simulation technique (6–8), a direction from one random point to another is isotropically distributed in a 3-D space but accounts for position of no other points. Earthquake point patterns clearly deviate from planar geometry: earthquake faults branch and form en-echelon patterns and other complex shapes (Kagan 1991a; Ben-Zion & Sammis 2003). On the other hand, the fractal point structure exhibits obvious anisotropy (Kagan 1981a;b); linear features in 2-D and planar in 3-D are good approximations. Kagan (1982) and Libicki & Ben-Zion (2005) created models of earthquake fault geometry that try to capture such features of earthquake fault geometry. However, here we use only simple geometrical patterns (Eqs. 5–8). Therefore, our derived corrections for the biases and other deficiencies of earthquake catalogs should be considered a first approximation.

3. Earthquake catalogs

Beginning in 1932, the CalTech (CIT) dataset (Hileman *et al.* 1973; Hutton & Jones 1993) was the first instrumental local catalog to include small earthquakes ($M \geq 3$). In recent years even smaller earthquakes have been included in the catalog. Presently the magnitude threshold is about 1.5 (Wiemer & Wyss 2000).

The catalog of relocated earthquakes (Richards-Dinger & Shearer 2000) contains 297,400 events for the period 1975-1998. These events have been relocated using spatially varying station terms to improve the accuracy of relative location. The median horizontal accuracy is 0.3 km and the vertical uncertainty is about 0.7 km. These values are significantly better then those for the CIT catalog, especially during its early period.

The another relocated catalog for southern California was produced by Hauksson & Shearer (2005) and Shearer *et al.* (2005). They applied waveform cross-correlation to obtain precise differential times between nearby events. These times can then be used to greatly improve the relative location accuracy within clusters of similar events. In many regions, this new catalog resolves individual faults in what previously appeared to be diffuse earthquake clouds (see Fig. 1 and Fig. 7 in Shearer *et al.* 2005).

Richards *et al.* (2006) compare traditional methods of earthquake location and discuss the advantages of modern new location methods and their application for California catalogs. They show that for these new methods the location uncertainty is ten to hundred times lower than for old catalogs based on seismic phase pick data.

The PDE (Preliminary Determination of Epicenters, 1999, and references therein) worldwide catalog is issued by the USGS (U.S. Geological Survey). The catalog contains more than 50,000 shallow earthquakes with $m_b \geq 5$ from 1965 to 2004/1/1.

4. Sources of error and bias in estimating the correlation dimension

There is an extensive bibliography on statistical estimation of the dimension (for example, Smith 1988; Nerenberg & Essex 1990; Ogata & Katsura 1991; Pisarenko & Pisarenko 1995; Eneva 1996; Vere-Jones *et al.* 1997; Vere-Jones 1999; Harte 1998, 2001; De Luca *et al.* 1999, De Luca *et al.* 2002; Molchan & Kronrod 2005, and references therein). However, these publications insufficiently consider the systematic effects which largely influence estimation of the fractal or scaling dimensions for earthquakes. Many of these publications consider methods for estimating correlation dimension with little quantitative discussion of various biases, which as we see later, may significantly alter the dimension value even if evaluated by a seemingly efficient statistical method. Some of the above publications estimated several effects using synthetic catalogs. As we discuss later in this Section, such simulations are insufficient for understanding various biases.

Smith (1988) and Nerenberg & Essex (1990) considered boundary effect by calculating the correlation dimension for a hypercube or a hypersphere. These region geometries are not often encountered in earthquake statistics. De Luca *et al.* (1999; 2002) investigated boundary bias and location errors influence by simulation. Harte (1998, p. 602, see also Harte 2001, his Section 11.3) discusses several effects that may cause bias in the correlation dimension estimates: "boundary effect, lacunarity, rounding effect, and noise or location error", but again these effects are only analyzed by simulation. We consider lacunarity or intermittency of spatial earthquake distribution as a natural consequence of its statistical self-similar pattern, for other biases analytic formulas are derived below to describe their influence.

These systematic effects are largely caused by geometrical factors. Many stochastic geometrical problems for point distribution in various figures are considered in http://mathworld.wolfram.com/topics/GeometricConstants.html (see also Wolfram 1999).

For some of these geometrical distributions we need to make assumptions which are not fully realistic. As a rule such assumptions are needed to obtain an analytic result. More general distributions can be obtained by simulations. However, theoretical expressions are still useful: firstly, they often are sufficient to understand the extent of an error or a systematic effect influence on results; secondly, the closed-form solutions are needed to check simulation programs which may contain hidden flaws. The theoretical expressions below are usually represented in a form accessible to computation by standard software packages: FORTRAN, MATLAB, and MATHEMATICA. We list these expressions below, starting with those affecting the estimate for small distances between events (see also Kagan & Knopoff 1980; Kagan 1991a).

4.1. The number of earthquakes in a sample

Clearly the δ-value cannot be determined for distances less than the smallest distance ($r_{\min}$) between points. Strictly speaking, the fractal dimension of a point set is zero (Vere-Jones 1999), but $\delta = 0$ for $r \leq r_{\min}$ and should increase for greater distances. Nerenberg & Essex (1990) call this effect 'depopulation' and estimate the critical minimum distance as

$$r_{\min} = 2R \times (1/N)^{1/D}, \quad (9)$$

where N is the number of points in the cube of size $2R$, and D is the dimension of embedding Euclidean space.

Modern earthquake catalogs contain thousands and tens of thousands of events. Thus, unless we are interested in the distribution of only the strongest earthquakes, samples are well 'populated'. The distribution of events at small distances may be influenced by having too few earthquakes. As we will see, this distribution is more likely strongly biased by other effects.

4.2. Earthquake location error

The location error randomizes earthquake locations and, as a result, the correlation dimension estimate δ approaches D for distances less than or comparable to the average location uncertainty. In early catalogs, earthquakes and especially aftershocks, were often assigned a common location and depth. This decision reduces the δ-value (an example is shown in Fig. 14 below).

We assume that earthquake location errors are normally distributed and that errors for both points are independent of each other. The obtained earthquake locations for close events are most likely influenced by similar biases hence they are not statistically independent. However, in this work we measure the pairwise distances between earthquakes, thus only relative errors influence the result.

The distribution of distance r between the two epicenters or hypocenters whose actual separation is ρ obeys a "non-central χ-distribution" (Fisher 1928; Kendall & Moran 1963, Chapter 5.19). Below we analyze this distribution for 3-D and 2-D earthquake spatial patterns (hypocenters and epicenters).

4.2.1. Earthquake location error: the 3-D case

Horizontal error is usually much smaller than vertical error. However, the general case of unequal errors cannot be analytically solved. If we assume for simplicity in a 3-D case that horizontal and vertical location errors are equal, the probability density of the 3-D non-central χ-distribution for hypocenters is

$$\phi(r|\rho) \;=\; \frac{r}{\rho\sqrt{2\pi}}\left[\exp-\frac{(r-\rho)^2}{2} \;-\; \exp-\frac{(r+\rho)^2}{2}\right] \quad (10)$$

Both distances r and ρ are scaled by σ. If $\rho \to 0$, the distance distribution becomes the Maxwell law, with probability density function

$$\phi(r) \;=\; r^2\sqrt{\frac{2}{\pi}}\exp\left(-\frac{r^2}{2}\right)\,. \quad (11)$$

The Maxwell law corresponds to the distribution of vector length in three dimensions, if the components of a vector are statistically independent and have a Gaussian distribution with the zero mean and the standard error σ. For large ρ distribution (10) becomes the Gaussian one (Fisher 1928, p. 664). The density is shown in Fig. 2.

If we assume that hypocenters are distributed over a fractal set with the dimension δ, then the number of events in a sphere of the radius R, centered on one of the points, i.e., the number of pairs in the 3-D space, $N_3(R)$, is

$$N_3(R) \;\propto\; \int_0^R dr \int_0^\infty \phi(r|\rho)\,\rho^{\delta-1}\,d\rho$$

$$= \frac{2^{\delta/2}}{\sqrt{2\pi}}\,\Gamma\left(\tfrac{\delta}{2}\right)\int_0^R r^2\,\exp\left(-\tfrac{r^2}{2}\right)\,{}_1F_1\left(\tfrac{\delta}{2},\tfrac{3}{2},\tfrac{r^2}{2}\right)\,dr\,, \quad (12)$$

where Γ is a gamma function and ${}_1F_1$ is the Kummer confluent hypergeometric function (Abramowitz & Stegun 1972; Wolfram 1999).

For $\delta = 3$ the function ${}_1F_1\left(\frac{3}{2},\frac{3}{2},\frac{r^2}{2}\right)$ is $\exp\left(\frac{r^2}{2}\right)$, and for $\delta = 2$

$${}_1F_1\left(1,\frac{3}{2},\frac{r^2}{2}\right) \;=\; \frac{1}{r}\sqrt{\frac{\pi}{2}}\,\exp\left(\frac{r^2}{2}\right)\,\mathrm{erf}\left(\frac{r}{\sqrt{2}}\right)\,, \quad (13)$$

where $\mathrm{erf}(R)$ is an error function. Then

$$N_3(R) \;\propto\; \int_0^R r\,\mathrm{erf}(r)\,dr$$

$$= \; R\sqrt{\tfrac{2}{\pi}}\times\exp\left[-R^2/2\right] + \mathrm{erf}\left(\tfrac{R}{\sqrt{2}}\right)\left[R^2-1\right]. \quad (14)$$

The ratio $RN_3(R)/V_R$ can be estimated as

$$RN_3(R)/V_R \;=\; \tfrac{2}{R^2}\,N_3(R)$$

$$= \; \sqrt{\tfrac{2}{\pi}}\times\frac{\exp\left[-R^2/2\right]}{R} + \mathrm{erf}\left(\tfrac{R}{\sqrt{2}}\right)\,\left[1-R^{-2}\right]\,, \quad (15)$$

where V_R is a sphere volume. For other values of the dimension δ, the integrals (12) and Eq. (20) below can be estimated numerically (Wolfram 1999).

Using (14) we estimate the correlation dimension for $\delta = 2$ in the presence of location errors as (4)

$$\hat{\delta} \;=\; \frac{\partial\left[\log N_3(R)\right]}{\partial\left(\log R\right)} \;=\; \frac{2\,R^2\,\mathrm{erf}\left(\frac{R}{\sqrt{2}}\right)}{N_3(R)}\,. \quad (16)$$

For large distances $\hat{\delta} \to 2$. For small values of the argument

$$\mathrm{erf}\left(\frac{R}{\sqrt{2}}\right) \;\approx\; R\sqrt{\frac{2}{\pi}}\times\exp\left[-R^2/2\right]\times\left[1+\frac{R^2}{3}\right] \quad (17)$$

(Abramowitz & Stegun 1972, Eq. 7.1.6). Hence putting (17) in (16), we obtain that for small distances $\hat{\delta} \to 3$.

In Fig. 3 we show the dependence of $\hat{\delta}$ on the distance, both for simulation and computation according to (16). In a synthetic catalog, we simulated 200,000 points on a 500×1000 km plane fault and then perturbed the location by adding the Gaussian errors. When calculating the $\hat{\delta}$-value, we compared the correlation function at distances separated by a factor $2^{1/4} = 1.189$.

4.2.2. Earthquake location error: the 2-D case

For the 2-D case of epicenters with location errors equal to σ, the non-central χ-distribution density is

$$\phi(r|\rho) \;=\; r\,\exp\left(-\frac{r^2+\rho^2}{2}\right)\,I_0\left(r\rho\right)\,, \quad (18)$$

where I_0 is the modified Bessel function of zero-th order. If $\rho \to 0$, the distance distribution becomes the Rayleigh law

$$\phi(r) \;=\; r\,\exp\left(-\frac{r^2}{2}\right)\,, \quad (19)$$

which is a distribution of vector length in two dimensions, (*cf.* Eq. 11).

As in the 3-D case, we assume that epicenters are distributed over a set with the fractal dimension δ. Then the number of the events measured over the Earth's surface in a circle of the radius R, again centered on one of the points, i.e., the number of pairs in the 2-D space, $N_2(R)$, is

$$N_2(R) \;\propto\; \int_0^R dr \int_0^\infty \phi(r|\rho)\,\rho^{\delta-1}\,d\rho$$

$$= 2^{\delta/2-1}\,\Gamma\left(\frac{d}{2}\right)\int_0^R r\,\exp\left(-\frac{r^2}{2}\right)\,{}_1F_1\left(\frac{\delta}{2},1,\frac{r^2}{2}\right)dr\,, \qquad (20)$$

see (12).

For $\delta = 1$

$${}_1F_1\left(\frac{1}{2},1,\frac{r^2}{2}\right) \;=\; \exp\left(\frac{r^2}{4}\right)\,I_0\left(\frac{r^4}{4}\right), \qquad (21)$$

and for $\delta = 2$

$${}_1F_1\left(1,1,\frac{r^2}{2}\right) \;=\; \exp\left(\frac{r^2}{2}\right). \qquad (22)$$

In Fig. 4 we show the dependence of $\hat{\delta}$ on the scaled distance for hypocenters or epicenters displaced by the Gaussian errors with the standard deviation σ. We compute $\hat{\delta}$ according to (12) and (20). There is little difference between these curves as the underlying dimension of the point pattern changes. In the 2-D case, however, the curves are slightly displaced toward smaller values of the scaled distance.

4.3. Projection effect for epicentral scaling dimension

Assuming, for example, that hypocenters cover a fault-plane ($\delta = 2$), the epicentral correlation dimension may fluctuate from $\delta = 1$ to $\delta = 2$, depending on the dip angle of a fault. Thus, for distances comparable to the thickness of the seismogenic zone, the correlation dimension value should depend on the style of the earthquake deformation pattern. In the general case, projecting a 3-D distribution onto a 2-D plane is called "grading" after Matheron (1971).

For illustrative purposes we have calculated the 2-D spatial moment, assuming both that the original seismicity was isotropic and the 3-D distance pair number function $N_3(R)$ is proportional to R^δ. Then a horizontal layer of seismicity of thickness W is projected on a horizontal plane:

$$\begin{aligned} G(R) \;&=\; RN_2(R)/(\pi R^2) \\ \propto\; (2/R)\int_0^R r\,dr\int_0^W (W-h)(r^2+h^2)^{(\delta-3)/2}\,dh\,. \end{aligned} \qquad (23)$$

This integral is a complex expression involving hypergeometric functions.

For integer δ simpler expressions can be found. For $\delta = 1$

$$G(R) \;=\; W\left[2\,\arctan\left(A^{-1}\right) - \tfrac{1-A^2}{A}\log\left(B\right) + A\log\left(A\right)\right], \qquad (24)$$

where $A = R/W$ and $B = \sqrt{1+A^2}$. For $\delta = 2$ we obtain the corrected Eq. 3 in Kagan & Knopoff (1980)

$$G(R) \;=\; W^2\left[\frac{B-1}{A} + A\log\frac{B+1}{A} - \frac{2\,(B^3-A^3-1)}{3\,A}\right]. \qquad (25)$$

And for $\delta = 3$

$$G(R) \;=\; W^3\,\frac{A}{2}\,, \qquad (26)$$

i.e., in this case the ratio (or an estimate of the correlation dimension) does not depend on distance. This is expected since here projecting uniformly 3-D distributed hypocenters on a surface is again a uniformly 2-D distributed pattern.

Using expressions (24–26) we can calculate an estimate of the correlation dimension for the grading problem:

$$\hat{\delta} \;=\; 1 + \frac{\partial\,(\log G)}{\partial\,(\log R)}. \qquad (27)$$

In particular for $d = 1$

$$\hat{\delta} \;=\; \frac{2\,A\,\left[\arctan\left(\frac{1}{A}\right) - A\log\left(\frac{B}{A}\right)\right]}{2\,A\,\arctan\left(\frac{1}{A}\right) - A^2\log\left(\frac{B}{A}\right) + \log(B)}\,, \qquad (28)$$

for $d = 2$

$$\hat{\delta} \;=\; A^2\,\frac{2\log\left(\frac{1+B}{A}\right) + \frac{6A-4B-3}{3} + \frac{1+B-2A^2B+A^2}{3B(1+B)}}{A^2\log\left(\frac{1+B}{A}\right) + \frac{2A^3-1+B(1-2A^2)}{3}}\,, \qquad (29)$$

and for $d = 3$

$$\hat{\delta} \;\equiv\; 2\,. \qquad (30)$$

In Fig. 5 we show the dependence of $\hat{\delta}$ on the distance scaled with the width of a seismogenic layer (W). Three distributions of the points are assumed in the layer: with $\delta = 1$; $\delta = 2$; and $\delta = 3$ (i.e., uniform Poisson distribution). The correlation dimension is determined for the projection of the points on a horizontal plane (equivalent to the epicenters). We display both theoretical values of the dimension (Eqs. 28, 29, 30, respectively) and the simulated values again evaluated at distances separated by a factor $2^{1/4}$.

The curves show the expected behavior: for small scaled distances $\hat{\delta} \;\to\; \delta - 1$ as the result of projection (Mandelbrot 1983), but for large distances $\hat{\delta} \;\to\; \delta - 2$. For the Poisson point distribution in a layer, the point pattern projected on a surface has a uniform $\hat{\delta} \;= 2$.

4.4. Boundary effects

For practical measurements when the size (diameter) of the set explored exceeds the distance r, the correlation function stops increasing. Nerenberg & Essex (1990) call this effect 'saturation' and estimate the critical minimum distance as

$$r_s = R/(D+1)\,. \qquad (31)$$

As in (9) $2R$ is the side of a cube and D is the embedding dimension. If $r > r_s$ in the correlation function $C(r)$, the function is saturated: its value does not represent the scaling effect of a point pattern.

For local and regional earthquake catalogs, the spatial boundaries delineate the area of sufficient coverage. For distances comparable to the area size, the δ-value estimate is biased depending on how the fault system pattern relates to the area polygon. If, for example, a narrow rectangular box were oriented along the direction of the major faults or perpendicular to them, this bias would significantly differ.

Below we consider a few simple cases where $\hat{\delta}$ can be analytically derived. The distribution of the distances in more complicated polygons and other figures can be obtained by a simulation.

4.4.1. Boundary effects: a 2-D case

The simplest 2-D figure is a disk. For points in a disk of diameter d, the distribution density for normalized distance $y = r/d$ between two random points inside is (Hammersley 1950)

$$\phi(y) \;=\; \frac{16\,y}{\pi\,d}\left[\arccos(y) - y\sqrt{1-y^2}\,\right]. \qquad (32)$$

The surface area for the box in Fig. 1 is $S \approx 233,300$ km^2. Approximating it by a circle, we obtain its radius as 272.5 km. When calculating temporal correlation functions, 10% of the time interval is usually considered the upper limit for reliable estimation. In southern California this would suggest that for distances over 25–50 km, the $\hat{\delta}$ values are more questionable.

Garwood (1947) and Ghosh (1951) propose formulas to calculate the distribution density for distances r between random point pairs in a rectangular box $a \times b$ for $a > b$:

$$\phi_1(r) = \frac{2\,r}{a^2\,b^2}\left[a\,b\,\pi - 2\,r\,(a+b) + r^2\right] \quad \text{for } r \le b\,, \tag{33}$$

$$\phi_2(r) = \frac{4\,r}{a^2\,b^2}\left[a\sqrt{r^2-b^2} - \frac{b^2}{2} - a\,r + a\,b\,\arcsin\left(\frac{b}{r}\right)\right] \quad \text{for } b < r \le a\,, \tag{34}$$

and

$$\phi_3(r) = \frac{4\,r}{a^2\,b^2}\left[a\sqrt{r^2-b^2} + b\sqrt{r^2-a^2} - \frac{1}{2}\left(a^2+b^2+r^2\right) - a\,b\,\arccos\left(\frac{a}{r}\right) + a\,b\,\arcsin\left(\frac{b}{r}\right)\right], \tag{35}$$

for $a < r \le \sqrt{a^2+b^2}$.

4.4.2. Boundary effects: 3-D case

Here, we discuss a distribution of distances in a horizontal layer of width W in a 3-D space. This would correspond to the average number of hypocenter pairs within a distance R of an arbitrary point in a layer of uniformly distributed seismicity. Three cases need to be considered: a sphere of radius R not touching any layer boundary, a sphere intersecting only one boundary, and another intersecting both boundaries.

For various distance ranges, we obtain three expressions. For $R < W/2$

$$N_3(R) = \frac{4\,\pi\,(W-2R)\,R^3}{3W} + \frac{2\,\pi}{3W}\int_0^R (2\,R-h)\,(R+h)^2\,dh = \frac{\pi\,R^3}{6W}\,(8\,W - 3\,R)\,. \tag{36}$$

For $W > R > W/2$ as in (36)

$$N_3(R) = \frac{2\pi}{3}\int_0^{W-R}(2\,R-z)\,(R+z)^2\,dz + \frac{2\pi}{3}\int_{W/2}^{R}\left[4\,R^3 - (R-z)^2\,(2\,R+z) - (W+2\,R-z)\,(R-W+z)^2\right]dz = \frac{\pi\,R^3}{6W}\,(8\,W-3\,R)\,. \tag{37}$$

For $R > W$

$$N_3(R) = \frac{\pi}{3W}\int_0^W\left[4\,R^3 - (R-h)^2\,(2\,R-h) - (W+2\,R-h)\,(R-W+h)^2\right]dh = \pi\,W^2\left(R^2 - \frac{W^2}{6}\right)\,. \tag{38}$$

For $R < W$ the estimate of correlation dimension is

$$\hat{\delta} = \frac{12\,(2\,W - R)}{8\,W - 3\,R} = \frac{12\,(2-\rho)}{8-3\,\rho}\,, \tag{39}$$

where $\rho = R/W$. For $R > W$ it is

$$\hat{\delta} = \frac{2\,R^2}{R^2 - W^2/6} = \frac{2\,\rho^2}{\rho^2 - 1/6}\,. \tag{40}$$

As expected, for $\rho \to 0$ the hypocentral correlation dimension estimate $\hat{\delta} \to 3$ and for $\rho \to \infty$ the dimension $\hat{\delta} \to 2$.

4.5. Inhomogeneity of earthquake depth distribution

Inhomogeneity of earthquake depth distribution influences the hypocentral fractal dimension. If this distribution were in fact uniform over depth, the dimension estimate would approach the real δ-value for distances smaller than the thickness of the seismogenic zone (see Eqs. 39–40). Otherwise, the apparent dimension value is effectively a convolution of the scale-invariant distribution with a non-uniform depth distribution.

We correct the hypocentral moment for the non-uniformity of the earthquake depth distributions:

$$G(R) = R N_2(R)/(\pi R^2) \propto (2/R)\int_0^R r\,dr\int_0^r K(z)\,(r^2+z^2)^{(\delta-3)/2}\,dz\,. \tag{41}$$

Here, $K(z)$ is the depth covariance function

$$K(z) = (\Delta h)^{-2}\int_{h_1}^{h_2} N(h,\,h+\Delta h)\,N(h+z,\,h+z+\Delta h)\,dh, \tag{42}$$

where $N(h,\,h+\Delta h)$ is the number of hypocenters in Δh depth interval, h_1 and h_2 are depth limits: for example, for global shallow seismicity, $h_1 = 0$ and $h_2 = 70$ km. The integrals in equations (41) and (42) can be evaluated numerically for a known distribution $N(h)$. The similarity between (23) and (41) is not accidental, since $C\,(W-h)$ is a correlation function (C is a normalizing coefficient) for the number of hypocenters in a layer W, if hypocenters are distributed uniformly over depth.

In Fig. 6 we display the distribution of the hypocenter numbers for the Hauksson & Shearer (2005) catalog as well as the correlation function (42). We used the magnitude threshold $M_c = 3$, since the depth accuracy of these earthquakes should be higher. Most of the correlation function can be approximated by a linear function $C\,(W-h)$ with $W = 13.5$ km.

For $d = 3$, i.e., the Poisson 3-D distribution of hypocenters with depth density $N(h,\,h+\Delta h)$, the pair number distribution is

$$N_3(R) = \frac{4\pi}{S}\int_0^R r\,dr\int_0^r K(z)\,dz\,, \tag{43}$$

where S is the surface area spanned by a catalog. Putting $K(z) = C\,(W-z)$ in (43), corresponding to a covariance function for a layer with uniform seismicity, we recover (36). For distances longer than $W/2$, the covariance function can be padded by zeros. Thus, we do not need to calculate more complicated formulas (37) and (38).

In Fig. 7 we show two curves to account for depth inhomogeneity. One is based on the depth correlation function (43); another uses Eqs. (36–38) to calculate pair numbers in a layer with width 13.5 km. As Fig. 6 demonstrates, the

correlation function of the hypocentral depth distribution is well approximated by a linear fit. Hence, both curves in Fig. 7 almost coincide.

In this figure as well as in several subsequent plots (Figs. 8, 9, 11) we scale the number of earthquake pairs N_D by dividing the number by distance R or by its square R^2. This is done to reduce the size of the plots and simplify them.

It may seem from Fig. 7 that we can correct for depth inhomogeneity without Eqs. 41–43. However, the depth distribution in other earthquake catalogs may be more difficult to approximate by a uniformly distributed point pattern. For example, in global catalogs of shallow earthquakes, many events are assigned the depth of 10 and 33 km, making the covariance function highly 'spiky'.

4.6. Earthquake pattern depth influence

Earthquake depth influences the degree of seismic coupling: it determines which part of the tectonic deformation is released by earthquakes. Apparently, for shallow subduction and continental earthquakes, the coupling coefficient is close to 1.0 (McCaffrey 1997; Bird & Kagan 2004). For deeper earthquakes, most of the tectonic motion is accommodated by plastic deformation (Kagan 1999). In global catalogs deep earthquake locations are more clustered than those of shallow seismicity, and the δ-value decreases (see Kagan & Knopoff 1980; Kagan 1991a, and Fig. 18 below).

Wyss *et al.* (2004) attempted to determine the correlation dimension for shallow earthquakes in a creeping section of the San Andreas fault near Parkfield. They found that the spatial earthquake distribution shows no scale-invariant distance range. Hence the $\hat{\delta}$-value is not well defined for this region.

4.7. Temporal influence

For small time intervals, earthquakes are more clustered and their correlation dimensions are smaller (Kagan 1991a; Helmstetter *et al.* 2005). This is perhaps the most important issue influencing the δ-value estimate. The previous items in this Section influence the estimate for a limited distance range only and hence can be recognized and compensated, or alternatively these distance ranges can be ignored in the correlation dimension calculation. However, time dependence extends over all distance intervals and cannot be that easily corrected.

We have estimated the distribution of distances between hypocenters $N_3(R)$, using the Hauksson & Shearer (2005) catalog (Section 3). We have selected only $M \geq 2$ earthquakes relocated with an accuracy of ϵ_h (horizontal) and ϵ_z (vertical) smaller than 0.1 km. In the catalog, there are 82442 $m \geq 2$ earthquakes in the time period [1984, 2002], out of which 33676 (41%) are relocated with $\epsilon_h < 0.1$ km and $\epsilon_z < 0.1$ km (see also Helmstetter *et al.* 2005, their Figure 5).

The distance number function of $N_3(R)$ between the hypocenters is close to a power-law $N_3(R) \propto R^{\delta}$ in the range $0.1 \leq R \leq 5$ km. The correlation fractal dimension (measured by least-square linear regression of $\log(R)$ and $\log[N_3(R)]$ for $0.1 \leq R \leq 5$ km) is $\hat{\delta} \approx 1.5$ (black lines in Figures 8 and 9). The faster decay for $R < 0.1$ km is due to location errors (Section 4.2.1), and the roll-off for distances $R > 5$ km is due to the finite thickness of the seismogenic crust (Section 4.4.2). For larger distances ($R > 50$ km), the $\hat{\delta}$ decrease is caused by catalog boundaries (Section 4.4.1).

To estimate the time dependence of the spatial distribution of inter-event distances, we have measured the distribution $N_3(R,t)$, using only earthquake pairs with an inter-event time τ in the range $[t,\ t+dt]$ (Fig. 8). We have also computed the distribution

$$N_3(R, \tau \geq t) \ = \ \int_t^T N_3(R,t')dt' \,, \qquad (44)$$

cumulated over all times larger than t (only using events with inter-event times larger than t up to $T = 2500$ days, see Fig. 9).

As the minimum inter-event time increases, the fraction of small distances will decrease. For inter-event times larger than 1000 days, the fractal dimension of the cumulative distribution $N_3(R, \tau \geq t)$ increases with t from the value measured for the whole catalog ($\hat{\delta} \approx 1.5$) to a maximum value close to 2. For $N_3(R,t)$, $\hat{\delta}$ increases between $\hat{\delta} \approx 0$ at times $t = 5$ minutes up to $\hat{\delta} \to 2$ for $t = 2500$ days (Fig. 10). This maximum inter-event time of 2500 days is long enough so that earthquake interactions are relatively small compared to the tectonic loading. Only an insignificant fraction of earthquake pairs are triggering-triggered events. This value $\hat{\delta} = 2$, measured for $t = 2500$ days, can thus be interpreted as approaching the fractal dimension of the active fault network.

However, Fig. 10 clarifies that $\hat{\delta} \to 2$ is not an asymptotic limit for the correlation dimension. The $\hat{\delta}$-value continues to increase. The time interval for the Hauksson & Shearer (2005) catalog (1984-2002) is too short for the $\hat{\delta}$ to reach the final value. As we mentioned earlier, in a local catalog the seismicity pattern for larger time intervals is strongly influenced by a few strong earthquakes and their aftershocks (Section 1).

The results for global catalogs yield a better measure of the asymptotic $\hat{\delta}$-value. In such cases the range of the correlation dimension change is also large. For shallow earthquakes, $\hat{\delta}$ varies from 1.2 to 2.1 (Table 2 in Kagan 1991a) for time intervals of 1.0-8575 days. Furthermore, whereas the results shown in Figs. 8–10 may be explained by a strong spatial concentration of aftershocks for several large Californian earthquakes, Figs. 2 and 3 in Kagan (1991a) demonstrate that this temporal effect is present in the PDE global catalog, both the original and declustered one.

The great variability of the $\hat{\delta}$-value with time intervals is important. Whereas previous items (in Sections 4.1–4.6) are discussed in spatial analyses of earthquake patterns (see references in the Introduction section), little is done to address the temporal aspect. Most likely, the full statistical analysis of this problem would require taking into account tectonic and seismic deformation rate in various types of plate boundaries (Bird & Kagan 2004).

The strong dependence of the correlation dimension on time contradicts the widely used Aki's (1981) hypothesis of connection between the b-value of the Gutenberg-Richter law (Bird & Kagan 2004) and the δ-value. Indeed, the b-value is largely independent of time (Kagan 2004). In some publications (Wyss *et al.* 2004, and references therein) it is suggested that the b-value can vary by a factor 1.5-2, but this change is not proposed for different time intervals but rather for various spatial and tectonic regions. However, even such b-value fluctuations cannot be matched by a strong variation of the δ-value (see above). Hence, the b-value cannot define the temporally dependent earthquake fractal spatial dimension (see also discussion by Kagan 1991b, p. 132).

4.8. Randomness

Finally, we mention the randomness of earthquake occurrence. Even when all other effects are taken into account, earthquakes occur randomly in time and space.

Moreover, because of earthquake clustering, especially the short-term which expresses itself in foreshock-mainshock-aftershock sequences, the effects of randomness are stronger than for a Poisson process (Vere-Jones 1999). Local catalogs often contain large aftershock sequences which make up a significant part of the total. Therefore, though such catalogs list many thousands of earthquakes, the effective size of a sample may amount to a much fewer events. Consequently, random fluctuations can be quite strong. An example of such a gross fluctuation is shown in Fig. 12.

5. Correlation dimension for earthquake catalogs

5.1. Corrections for errors and biases

In this subsection we use the results of Section 4 to take into account and sometimes correct the observed distance distributions.

5.1.1. Example

Fig. 11 displays the spatial hypocentral and epicentral moment curves for the Hauksson & Shearer (2005) catalog (Section 3). The distance scale is increased by a factor of $2^{1/4}$, starting with $R = 0.01$ km. In Fig. 12 we show the estimate of the correlation dimension $\hat{\delta}$, calculated by a formula equivalent to (16). At the distances $R < 0.1$ km, random scatter (Section 4.8) dominates the pattern, although the relatively high values of average $\hat{\delta}$ can be clearly attributed to location errors (Section 4.2). The location error effects would be strong for distances $0.01 < R < 1.0$ km (in this subcatalog we did not delete the earthquakes with low location accuracy, as was done in Figs. 8–10). For distances approaching 10–15 km, the finite thickness of the seismogenic zone strongly influences the hypocentral dimension (Section 4.4.2 and Fig. 7).

The epicentral $\hat{\delta}$-value is close to 2.0 for small distances. This is likely due to the location errors (Fig. 4) and projection (Fig. 5), although the latter effects should be relatively small since most faults in southern California are almost vertical.

The difference between the hypocentral and epicentral correlation dimensions at larger distances (1–10 km) is due mostly to projection effects (Section 4.3). From Fig. 5 we see that for isotropic point distribution with $\delta = 2$, the epicentral correlation dimension should decay from $\hat{\delta} = 1.5$ to $\hat{\delta} = 1.0$ in the scaled distance range $R/W = [0.1 - 10.0]$. If earthquakes were distributed on vertical faults, the difference between the two dimensions would be exactly 1.0 ($\hat{\delta}_h = 2.0$, $\hat{\delta}_s = 1.0$) and independent of distance. (Here δ_h is the correlation dimension for the hypocentral moment and δ_s is the dimension for the epicentral one.) For the horizontally dipping faults both dimensions would be the same. In the California catalogs the spatial earthquake distribution mixes the above-mentioned patterns with a prevalence of vertical strike-slip faults. Thus, in Fig. 12 the difference between the dimensions is on the order of 0.5, and both dimensions decay with distance.

For distances exceeding the effective thickness of the seismogenic layer ($W = 13.5$ km), the epicentral and hypocentral moments practically coincide (see Section 4.5). Random fluctuations associated with aftershock clusters of a few major earthquakes again predominate at larger distances. Finally, for distances approaching the size of the box in Fig. 1 (hundreds km), the spatial boundary effects (see Section 4.4.1) strongly decrease correlation dimension.

5.1.2. Corrections and normalizations

We consider how the spatial moments can be corrected for the effects discussed in Section 4. Location errors are obvious targets for such a correction. Unfortunately, although these errors are studied extensively and many catalogs contain internal estimates of such uncertainties based on the discrepancy in fitting the arrival times, there are many difficulties in applying our expressions (Section 4.2). The internal errors are only part of the total location uncertainties, as we see in analyzing the earthquake catalog accuracy (Kagan 2003). Real location errors, including systematic ones, are often significantly higher.

Location errors vary over the time span and territory of catalogs. This is especially true for local catalogs. Catalogs based on the waveform cross-correlation have a high relative location accuracy for earthquake clusters where such correlation is feasible. However, for different clusters, associated relative error may be significantly higher.

To save effort and the paper size, we refrained in this work from correcting location errors and projection effects. Such procedures can be implemented in future studies of earthquake spatial distributions.

In Fig. 13 we show the epicentral and hypocentral curves for the Hauksson & Shearer (2005) catalog (Section 3), normalized by dividing $N_2(R)$ and $N_3(R)$ numbers by the appropriate pair numbers in a Poisson process. For the 2-D pattern, Poissonian epicenters are randomly distributed inside the box shown in Fig. 1. For distances comparable to the box size, we estimate the distribution of pair numbers, $N_2^p(R)$, using simulated catalog (cyan curve in Fig. 13). To avoid random fluctuations, when distances are small, we calculate

$$N_2^p(R) \;=\; \frac{N(N-1)}{2} \times \frac{\pi R^2}{S}\,, \qquad (45)$$

where S is the area of the box, and N is the number of points in a catalog. We combine both simulated and theoretical curves at $R = 3$ km.

The normalized epicentral curve in Fig. 13 is the ratio

$$N_2^n(R) \;=\; \frac{R}{R_{\max}} \times \frac{N_2(R)}{N_2^p(R)}\,, \qquad (46)$$

where $R_{\max} = 734.5$ km is the maximum distance in the box, and multiplication by $R/R_{\max}$ is done to make the curve approximately horizontal for $\delta_s = 1$ and to normalize the value of the moment at the maximum distance.

A similar normalization is carried out for the hypocentral moment. For small distances, we compute $N_3^p(R)$ using (43). We multiply the ratio of the observational curve to the Poisson one by $R/R_{\max}$, as in (46). Since the Poisson pattern has the dimension 3 here, the horizontal curve means that the hypocentral distribution has $\delta = 2$. The curves below the horizontal line have $\delta \geq 2.0$ (the fractal dimension is equal to the tangent of the slope angle of the curve plus 2.0). In one plot we combine two types of curves, epicentral and hypocentral, to show their difference.

The described normalizations rectify for the boundary effects. In the 2-D case, the correction relates to the box boundaries; in the 3-D case the bias due to the inhomogeneity of the depth distribution is also corrected. However, as we explained in Section 4, these corrections make certain assumptions about the actual spatial distribution of earthquakes. It is not clear whether these assumptions are fully valid. However, when comparing Fig. 11 to Fig. 13 where the corrections are applied, we see that such corrections increase the range of the scale-invariant behavior of the moments. The normalization, applied in Fig. 13, is used in all subsequent diagrams (Figs. 14–18). Similarly, in these diagrams the corrections extend the power-law moment range.

5.2. California catalogs

Figs. 14 and 15 display the spatial moment curves for the CalTech (CIT) catalog (Hileman *et al.* 1973) in two periods: 1932-2001 and 1975-2001. The curves' behavior for small distances demonstrates the influence of location errors and catalog compiling procedures. In the first plot for distances smaller than 3 km, the fractal correlation dimension is less than 1.0. The most likely reason for this is that during the first years of the CalTech catalog, the aftershocks were often assigned the same location as the mainshocks (see Section 4.2). This choice makes the dimension of an aftershock sequence equal to zero. Because many sequences are present in this catalog, the combined dimension is small, while not being a zero.

In the second plot (Fig. 15), only recent earthquakes have been processed. The correlation dimension for small distances (0-5 km) is close to 3.0. This value results from location errors which randomize the position of hypocenters and from projection effects (see Section 4.2).

Both curves' behavior at large distances (more than 100-200 km) is controlled by box boundary effects (see Section 4.4). In these plots we did not account for such effects as we had in Fig. 13. The scale-invariant part of the curves is in a distance range of 2-200 km, where the correlation dimension is slightly over 2.0. As explained in Section 4.8, the curves' fluctuations are probably caused by large aftershock sequences of the 1992 Landers, 1994 Northridge, and 1999 Hector Mine earthquakes.

Fig. 16 displays similar spatial distribution for the catalog of relocated earthquakes (Richards-Dinger & Shearer 2000). The higher location accuracy of these events is seen in the extension toward smaller distances of the scale-invariant region. Whereas the time span in both diagrams (Figs. 15 and 16) is approximately the same, the hypocentral moment in the latter plot extends as a power-law from about 0.5 km up to 200 km. The difference between the epicentral and hypocentral curves is larger for the Fig. 16 diagram. This is due to a higher accuracy of hypocentral solutions. If the vertical errors were comparable to the thickness of the seismogenic zone, the curves would be almost identical for distances comparable to the thickness (Kagan & Knopoff 1980).

Fig. 13 displays similar spatial distribution curves for the waveform cross-correlation catalog by Hauksson & Shearer (2005). The clusters of earthquakes in the catalogs have been cross-correlated to obtain relative accuracy on the order of tens of meters. Two distance regions can be seen in the curves: 0.2-20 km and 20-200 km. Apparently the catalog has two earthquake populations: one corresponding to the events in the cross-correlation clusters and the other to the inter-cluster distances. The first part ($R = 0.01 - 0.2$ km) of the hypocentral curve indicates that the earthquake spatial distribution behavior is controlled by location errors.

In Figs. 13, 14, 15, and 16, location accuracy generally improves over time and in later catalogs it improves as one employs more sophisticated interpretation of seismograms. We see that the range of statistical scale-invariant behavior is shifted towards smaller distances. In a complete CIT catalog (Fig. 14) which includes early location results, the implied average error is on the order of 3-5 km. In the later part of the catalog (Fig. 15), the hypocentral moment's scale-invariant part starts at about 1 km. For the newer catalogs (Figs. 16 and 13) the curves' scale-invariant behavior extends to 0.5 and 0.2 km, respectively. On the other hand, we see that the later catalogs exhibit more fluctuations at larger distances, due probably to aftershock clusters of a few large earthquakes.

To demonstrate the influence of the event temporal clustering, in Fig. 17 we show spatial distribution for the year 1994, the year of the Northridge, California earthquake (Thio & Kanamori 1996). The δ_h-dimension for the distance interval 20-200 km is close to 1.0. Most southern California seismicity for this period is concentrated in the Northridge focal zone; hence the scaling dimension for the larger distances is low. For the distance interval 2-20 km, the δ-value is approximately the same as in Figs. 14 and 15. This distance range roughly corresponds to the size of the Northridge earthquake rupture zone.

5.3. Global catalog

Fig. 18 displays epicentral and hypocentral moments for earthquakes in the worldwide PDE catalog (Section 3) at three depth intervals. The curves are calculated for the maximum time interval between events (37 years). We include all pairs of earthquakes without taking the inter-earthquake time into account.

Similar to (46) we plot the ratio for the epicentral curve

$$N_2^n(R) \;=\; \frac{2\,N_2(R)}{N\,(N-1)\,\sin^2\left[R/(2\,R_E)\right]} \times \frac{R}{\pi\,R_E}\,, \quad (47)$$

where R_E is the Earth radius. The hypocentral curve is normalized, using an expression similar to (43).

Epicentral moments yield a higher value of the exponent for distance ranges which are less than, or comparable to, the thickness of the appropriate layer (see Fig. 18). For the hypocentral moment, we normalize the pair numbers by dividing them by the appropriate numbers in a Poisson catalog in which earthquakes are distributed uniformly over the surface with the same depth distribution as in a real catalog (Kagan & Knopoff 1978; 1980) (see Eq. 43).

Fig. 18 demonstrates that for shallow earthquakes the hypocentral curves are approximately power-law in the distance interval 20-2000 km. But the epicentral curves exhibit a clear transition in their slope at distances corresponding roughly to the thickness of a seismogenic layer. Kagan & Knopoff (1980) showed that the lower distance range of the linearity breakdown (20 km) is explained by location errors, both horizontal and vertical.

The upper cutoff for scale-invariance (2000 km) is connected to the size of major tectonic plates (Kagan & Knopoff 1980; Kagan 1991a). For these distances, statistical self-similarity of the earthquake spatial distribution breaks down. The δ values in Fig. 18 demonstrate that the dimension decreases as the depth increases.

The value of the fractal dimension declines to 1.8-1.9 for intermediate events (depth interval 71-280 km) and to 1.5-1.6 for deeper ones. We see that epicentral and hypocentral curves converge at the distances equal to the thickness of a layer in which earthquakes are selected, the difference between the curves is a consequence of the projection effect and transition from 3-D to 2-D when the distance R increases (Sections 4.3–4.5).

Harte (1998) determined correlation dimensions for shallow and intermediate events in New Zealand. The estimates of the hypocentral correlation dimension (see Table 11.1 in Harte 2001) for deeper earthquakes (1.8–2.2) is slightly higher than for shallow events (1.7–1.9). The larger values of the dimension for intermediate events are, most likely, caused by location errors. As we mentioned in the Introduction, earthquakes registered by seismic networks situated on island chains can have large location errors, and these errors would increase for deeper events. Harte (1998, p. 616; 2001, p. 213) acknowledges that such an explanation is possible.

5.4. Comparison to tectonic plate size distribution

The distribution of the areas in steradians for large tectonic plates has been studied by Bird (2003, his Fig. 19). Sornette & Pisarenko (2003) investigated the distribution, using Bird's preliminary results. Bird found that the distribution for 52 plates has two branches: a scale-invariant for small plates with a power-law index $\mathcal{D} = 0.33$ and a rapidly decaying tail for large plates. The results obtained by Sornette & Pisarenko (2003) are similar: for 42 plates their fractal exponent value is 0.25.

Clearly, it would be more difficult to unambiguously identify even smaller plates: their statistics would not be complete and the 3-D deformation pattern would need to be considered for plates whose size is comparable with the thickness of a seismogenic layer.

The evidence presented in this Section indicates that for earthquake catalogs the appropriately scaled distribution has two branches: scale-invariant for small distances from zero up to 2000-3000 km, and a non-fractal, long-distance

tail (3000-20,000 km). As Fig. 18 demonstrates, the fractal (correlation) dimension (δ) is about 2.2 for shallow earthquakes (also see Kagan 1991a).

Kagan & Knopoff (1980, their Figure 11) obtained the correlation dimension estimate for tessellation of a sphere by three regular cubic (with triple junctions) polyhedra. The correlation dimension for small distances (0-3000 km) is 1.0 (or 2.0, if one takes depth into account). A transition to the large-range pattern occurs at about 2000-5000 km, depending on the polyhedron used. The small-range dimension value corresponds to the long edges of the regular polyhedra, close pairs of points more likely belong to the same cell edge.

For regular polyhedra tessellation, the plate distribution displayed like Bird's (2003, his Fig. 19) and Sornette & Pisarenko's (2003) diagram, would have a step-function at π, $2\pi/3$, and $\pi/3$ for the tetrahedron, the cube, and the dodecahedron, respectively. For small distances, the distribution exponent ($\mathcal{D}$) would be zero. If we introduce a scale-invariant distribution of plate sizes, the correlation dimension for earthquakes should increase. Why? In addition to long edges of large plates, the numbers of short-range point pairs would increase due to the branching edges (triple junctions) of the smaller plates. The question is how much it would increase the δ-dimension.

It would be interesting to match the two distributions (tectonic plates and earthquake locations) to see which fractal dimension exponent corresponds to the tectonic plates distribution. The only method that could be effectively applied to solve this problem is simulation. Plate formation could be represented as a Voronoi tessellation of a sphere. Many theoretical and computer studies exist for a Voronoi tessellation of a sphere based on the Poisson point distribution (Okabe *et al.* 2000). However, for our purposes a tessellation of power-law distributed plates needs to be developed. For instance, Nagel & Weiss (2005) propose a stochastic tessellation model for tensile cracks which has scale-invariant features.

The exponent $\mathcal{D}$ for a plate area S distribution should transform into $2\,\mathcal{D}$ for the distribution of plates linear size: $R \propto \sqrt{S}$. The fractal distribution of plate sizes should increase the correlation dimension for earthquake epicenters as $\delta_s = 1 + 2\mathcal{D}$ (and corresponding hypocentral dimension as $\delta_h = 2 + 2\mathcal{D}$). This would imply $\delta_h \to 2.6 - 2.7$. Furthermore, plates are not rigid. Most plates have significant intraplate seismic activity (Bird & Kagan 2004) which would increase the δ-value. The value $\delta_h = 8/3$ is then appropriate to the dimension of fluid turbulent flow (Mandelbrot 1983, p. 54).

As we discussed above (Section 4.7), estimates of the correlation dimension depend on the time span of a catalog. For a sufficiently long catalog, the δ-exponent should approach an asymptotic value (Kagan 1991a). The fractal exponent, $\mathcal{D}$, for the plate size distribution results from millions of years of plate tectonic evolution due to mantle convection. But the δ-value is determined for earthquake catalogs spanning a few decades. Therefore, on time scales of decades and centuries $\delta_h \to 2.2 - 2.3$ is probably an asymptotic value. It is possible that for longer times the correlation dimension would increase to $\delta_h = 2.6 - 2.7$.

Studying the earthquake magnitude distribution for shallow earthquakes in continental regions or their boundaries (Bird & Kagan 2004) yields estimates of the corner or maximum magnitude of the order $8.0 - 9.5$. These magnitude values indicate that rupture length for the largest earthquakes is a few hundred (500-1000) km: it is smaller than 2000–3000 km of the spatial scale-invariance breakdown (Fig. 18). This latter distance corresponds to the average size of the major continents or the total thickness of the mantle. Does it mean that the continent or tectonic plates formation is due to a full mantle convection? Does the stress which causes earthquakes accumulate only in the upper mantle of about 700 km thickness?

6. Discussion

Our major thrust has been to analyze errors and systematic effects influencing the estimate of the correlation dimension for spatial earthquake distribution. What can we say about the value of this dimension for the earthquake rupture process? We briefly review attempts to determine the fractal dimension for rock surfaces and earthquake faults.

6.1. Faults and rock surfaces

Ben-Zion & Sammis (2003) show examples of self-similar features of shear fault surfaces (their Fig. 3). They also discuss (their section 2.4) many measurements of scale-invariant features of fault traces, internal fault zone structures and fault networks (see also Kagan 1991a).

Bonnet *et al.* (2001) extensively discuss the properties of fractures at rock surfaces. The fractal dimension of the fault traces at the Earth's surface should be significantly influenced by a free boundary. Moreover, physical properties of the rocks near the surface should differ from rock properties at seismogenic depth. In particular, lithostatic pressure is zero at the surface. Consequently, tectonically stressed rock material would disintegrate, increasing the fractal dimension of the rock particles' distribution.

Schmittbuhl *et al.* (1995) and Amitrano & Schmittbuhl (2002) show that the fractal dimension of rock fracture surfaces is equal to 2.20-2.25. This dimension is determined for one surface. The earthquake fault system contains many fractally distributed surfaces, so their combined dimension may exceed the above value.

Weiss & Marsan (2003) studied spatial distribution of dislocations in an ice crystal. They obtained the correlation dimension estimate of 2.5 ± 0.1 for dislocation clusters, and noticed that close-in-time avalanches are more spatially clustered.

Repeating Mandelbrot's (1983, pp. 103-104) arguments, we suggest that $\delta \geq 2.0$, since any line connecting two blocks of material in shearing motion, would intersect at least one fault surface. The dimension of the embedding Euclidean space provides another limit on the value of δ: $3.0 \geq \delta \geq 2.0$. An ideal solid crystal (without defects) would fail along a planar dislocation ($\delta = 2.0$). However, since all natural rocks have defects, this would cause branching and bending of earthquake faults due to fault displacement incompatibility (King 1983; Gabrielov *et al.* 1996). Hence, the fracture correlation dimension would increase.

In general, rock fracture surfaces and exposed faults result from several processes. Hence their fractal dimension may not agree with that for earthquake spatial patterns. In the latter, we directly observe brittle fracturing rocks in situ; therefore, the correlation dimension is relevant to process of rupture. Furthermore, as discussed in Section 4, random and systematic errors of earthquake locations can be approximately evaluated. Such error estimates are more difficult to perform for earthquake faults and rock surface measurements.

6.2. Spatial fractal dimension: monofractal or multifractal?

Is the spatial distribution of earthquakes monofractal or multifractal (Molchan & Kronrod 2005)? In Section 4, we show that practically any value for the correlation dimension can be obtained if many errors and inhomogeneities in the observational data as well as deficiencies in data processing are not properly considered. Presently there are no similar estimates of systematic effects for multifractal measures of

the earthquake spatial dimension. Most likely the technical difficulties discussed in Section 4 are intensified for such multifractal measures.

In addition, as we discussed in the Introduction, certain methodological problems must be solved to evaluate multifractal dimensions for hypocentral distributions: the only exponents that have clear physical meaning. Moreover, these estimates need to be obtained for all scale-invariant ranges of spatial earthquake distribution: from distances close to zero to hundreds and thousands of km. Thus, it is doubtful that evaluating multifractal dimensions could yield significant results for presently available catalogs.

Perhaps a better insight into the spatial patterns of earthquake distributions could be obtained by analyzing higher order point configurations. Kagan (1981a;b) studied 3- and 4-point spatial moments for earthquake distribution. These moments correspond to point simplexes in 2-D and 3-D, respectively. Similar to the distance between two points, these sets have the advantage of being independent of any coordinate system and therefore lack the problems associated with box counting. The results of these studies suggest that these earthquake distributions are proportional to $1/S$ and $1/V$, where S is the area of a triangle and V is the volume of a tetrahedron formed by earthquake points. These geometrical patterns may provide important information on earthquake generation (see Section 6.4 below). A further way to study these multi-point patterns is to use the modern statistical and topological theory of shape (Small 1996; Kendall *et al.* 1999).

6.3. Spatial fractal dimension for earthquake rupture

What are the advantages and drawbacks of using local vs global earthquake catalogs for evaluating the correlation dimension? Local catalogs usually have highly accurate hypocenter solutions. The Hauksson & Shearer (2005) and Shearer *et al.* (2005) catalog has uncertainties much smaller than the thickness of the seismogenic layer. This high accuracy, as illustrated in Figs. 8–9, allows us to directly estimate $\hat{\delta}$ in 3-D and extend the scale-invariant part of the hypocentral moment close to zero distances (see Figs. 11–13). However, local catalogs have serious drawbacks: they are often strongly inhomogeneous in time and space. A few aftershock sequences usually dominate the long-range spatial distribution of events, and thus the spatial moment fluctuates strongly at large distances. As the result, $\hat{\delta}$ evaluation becomes difficult. Furthermore, because the high accuracy part of a catalog is of short span, the $\hat{\delta}$ estimates are strongly influenced by temporal effects.

Global earthquake catalogs have the advantage of more uniform coverage. They have no boundaries, allowing us to study spatial moments for large distances comparable to the Earth's size. However, location uncertainties are much higher in these catalogs compared to local ones. Thus, the moment behavior at small distances (up to 15-20 km) is controlled by location errors and projection effects. Therefore, the difference between the epicentral and hypocentral moments is small for worldwide catalogs (Fig. 18). However, we can observe scale-invariant behavior of the moments at a distance range of 20–2000 km and evaluate $\hat{\delta}$. Another advantage of global catalogs is their inclusion of many independent aftershock clusters. Their averaging produces much smoother curves at large distances.

However, in processing global catalog data, various tectonic regions are combined. Earthquake size statistics are different in these regions (Bird & Kagan 2004), and one may well expect that the spatial distribution pattern also varies. Since earthquakes in the subduction zones comprise about 52% of the total (*ibid*), global spatial distributions as in Fig. 18 are largely controlled by subduction earthquakes. In principle, we could subdivide the seismic regions into several categories (*ibid*) and analyze them separately. But, then we would have to work in a relatively constricted distance range between large location errors, specific for global catalogs, and relatively small sizes of tectonic regions.

Comparing spatial moments for various time spans and catalogs yields relevant conclusions about accuracy and the spatial properties of earthquake process. Therefore, we conclude that the statistical self-similarity of earthquake geometry is established down to the scale length of 0.5 km and less. Since the equations of elasticity do not have intrinsic scale, we expect that this property of spatial self-similarity can be extended for the brittle fracture of disordered materials (rocks) up to the scale of a few millimeters: the size of rock grains.

In this paper we focus on analyzing errors and systematic effects to determine the correlation dimension. Even if these biases are taken into account, the actual study of earthquake spatial patterns yields no reliable and converging estimates of the $\hat{\delta}$. Previous investigations (Kagan & Knopoff 1980; Kagan 1991a) suggest that the $\hat{\delta}$-value does not depend or has weak dependence on the magnitude threshold. However, the correlation dimension dependence on catalog time intervals (see Section 4.7) and the dimension for aftershocks of large earthquakes still need to be explored. Many systematic effects discussed in Section 4 make such investigations difficult.

Our analysis suggests that evaluating the fractal dimension for earthquake spatial patterns is difficult and prone to many errors and biases. This probably explains in contrast to two other classical statistical scale-invariant exponents of earthquake distribution: the Gutenberg-Richter relation (Bird & Kagan 2004) and Omori's law (Kagan & Houston 2005), which arguably are controlled by universal parameters, or by those with a slight variation, the properties and value of the correlation dimension are not yet agreed upon. We hope that the evidence presented here will persuade readers that the earthquake spatial distribution, at least in asymptotic time limit, has universal features also.

6.4. Earthquake fault geometry

Finally, we briefly discuss the conclusions that can be made on the basis of the results reported earlier, about the geometry of earthquake faults. If the correlation dimension is an integer the results are consistent with a simple geometrical model: a line in two dimensions and a plane in 3-D (Kagan & Vere-Jones 1996). Generally such a model is not acceptable since the δ-value is not an integer and because even cursory inspection of geologic maps or epicenter maps (such as Fig. 1) demonstrates that earthquakes occur on many faults.

Ben-Zion & Sammis (2003) argue that "to a good approximation, [hypocenters may reside] on a collection of Euclidean surfaces." It is certainly possible to approximate spatial earthquake distribution, which usually exhibits linear features in epicentral maps, by several planes. Such approximations may be even useful in comparing earthquake data with tectonic and geologic datasets. The approximations can be tested against two-point distance patterns studied in this paper to see to what degree they satisfy these distributions. However, it is clear that any finite number of planes would fail to fully describe earthquake spatial pattern. Inspecting, for example, Fig. 5 in Shearer *et al.* (2005) one can see that the number of required fault planes to would significantly increase as the accuracy of earthquake location improves.

In addition, the planar faults approximation is unlikely to have a predictive power: many large earthquakes in California, for example, like the 1952 Kern County, the 1992 Landers, or the 1999 Hector Mine, occurred on faults which had

little seismic activity before these events. On the other hand, estimates of the correlation dimension are robust, they yield approximately the same value, even when evaluated with a catalog without these events (Kagan & Knopoff 1980).

Moreover, the distribution of hypocenter quadruplets studied by Kagan (1981b) suggests that the planar geometry is only a first approximation for earthquake spatial distribution (see also Section 6.2). The distribution density of tetrahedra volumes (V) formed by these quadruplets is inversely proportional to tetrahedron's volume, fault planar geometry would imply the volume distributed as the delta function of V.

Ben-Zion & Sammis (2003) also suggest that the earthquake slip is usually localized in narrow planar zones. The branching stochastic models of earthquake geometry by Kagan (1982) and by Libicki & Ben-Zion (2005) predict such a behavior. The fault patterns simulated by these models also exhibit a quasi-planar deformation bands that are likely to be identified with a main trace of a fault. However, small or large planar faults occasionally branch off the main trace of a fault. Furthermore, these simulated faults are visually similar to real earthquake faults and they exhibit a statistically scale-invariant structure.

7. Conclusions

We briefly summarize our results and highlight their difference from similar investigations:

1. We provide closed-form expressions for most of systematic effects and random errors influencing estimates of the correlation dimension for earthquake spatial pattern. We test these formulae by simulation.

2. We evaluate the correlation dimension both for hypocentral and epicentral earthquake patterns and provide algorithms for comparison and mutual transformation of these two dimensions.

3. We estimate the correlation dimension for several local and global earthquake catalogs. Since these catalogs have different systematic and random biases and errors which influence the correlation dimension estimate, the reported results of the statistical analysis are more robust.

Acknowledgments. I appreciate partial support from the National Science Foundation through grants EAR 00-01128, EAR 04-09890, and DMS-0306526, as well as from the Southern California Earthquake Center (SCEC). SCEC is funded by NSF Cooperative Agreement EAR-0106924 and USGS Cooperative Agreement 02HQAG0008. The author thanks D. D. Jackson, A. Helmstetter, F. Schoenberg and I. V. Zaliapin of UCLA and D. Vere-Jones of Wellington University for very useful discussions. Agnès Helmstetter helped to construct Figures 8–10. Kathleen Jackson edited the manuscript. Publication 0000, SCEC.

References

Abramowitz, M. & Stegun, I. A., 1972. *Handbook of Mathematical Functions*, Dover, NY, pp 1046.

Aki, K., 1981. A probabilistic synthesis of precursory phenomena, in: *Earthquake Prediction, An International Review*, Maurice Ewing Vol. **4**, D. W. Simpson & P. G. Richards, eds., AGU, Washington, D.C., 566-574.

Amitrano, D. & J. Schmittbuhl, 2002. Fracture roughness and gouge distribution of a granite shear band, *J. geophys. Res.*, **107**(B12), ESE-19, 1-16, Art. No. 2375.

Bak, P., Christensen, K., Danon, L. & Scanlon, T., 2002. Unified Scaling Law for Earthquakes, *Phys. Rev. Lett.*, **88**, 178501 (pp. 1-4).

Ben-Zion, Y. & C. G. Sammis, 2003. Characterization of fault zones, *Pure Appl. Geophys.*, **160**, 677-715.

Bird, P., 2003. An updated digital model of plate boundaries, *Geochemistry, Geophysics, Geosystems*, **4**(3), 1027, doi:10.1029/2001GC000252.

Bird, P. & Y. Y. Kagan, 2004. Plate-tectonic analysis of shallow seismicity: apparent boundary width, beta-value, corner magnitude, coupled lithosphere thickness, and coupling in seven tectonic settings, *Bull. seism. Soc. Am.*, **94**(6), 2380-2399, see also http://element.ess.ucla.edu/publications/-2004_global_coupling/2004_global_coupling.htm

Bonnet, E., O. Bour, N. E. Odling, P. Davy, I. Main, P. Cowie & B. Berkowitz, 2001. Scaling of fracture systems in geological media, *Rev. Geophys.*, **39**, 347-383.

Daley, D. J., & Vere-Jones, D., 2003. *An Introduction to the Theory of Point Processes*, Springer-Verlag, New York, 2-nd ed., Vol. 1, pp. 469.

De Luca, L., S. Lasocki, D. Luzio & M. Vitale, 1999. Fractal dimension confidence interval estimation of epicentral distributions, *Annali di Geofisica*, **42**(5), 911-925.

De Luca L., D. Luzio & M. Vitale, 2002. A ML estimator of the correlation dimension for left-hand truncated data samples, *Pure appl. Geophys.*, **159**, 2789-2803.

Eneva, M., 1996. Effect of limited data sets in evaluating the scaling properties of spatially distributed data: An example from mining-induced seismic activity, *Geophys. J. Int.*, **124**, 773-786.

Fisher, R. A., 1928. General sampling distribution of the multiple correlation coefficient, *Proc. Roy. Soc. London*, ser. A, **121**, 654-673.

Gabrielov, A., Keilis-Borok, V. & Jackson, D. D., 1996. Geometric incompatibility in a fault system, *P. Natl. Acad. Sci. USA*, **93**, 3838-3842.

Garwood, F., 1947. The variance of the overlap of geometrical figures with reference to a bombing problem, *Biometrika*, **34**, 1–17.

Geilikman, M. B., T. V. Golubeva & V. F. Pisarenko, 1990. Multifractal patterns of seismicity, *Earth Plan. Sci. Letters*, **99**, 127-132.

Ghosh, P., 1951. Random distance within a rectangle and between two rectangles, *Bull. Calcutta Math. Soc.*, **43**, 17-24.

Hammersley, J. M., 1950. The distribution of distance in a hypersphere. *Ann. Math. Stat.*, *21*, 447-452.

Harte, D., 1998. Dimension estimates of earthquake epicentres and hypocentres, *J. Nonlinear Science*, **8**, 581-618.

Harte, D., 2001. *Multifractals: Theory and Applications*, Boca Raton, Chapman & Hall, 248 pp.

Harte, D., and Vere-Jones, D., 1999. Differences in coverage between the PDE and New Zealand local earthquake catalogues, *New Zealand J. Geol. Geoph.*, **42**, 237-253.

Hauksson, E. & P. Shearer, 2005. Southern California hypocenter relocation with waveform cross-correlation, Part 1: Results using the double-difference method, *Bull. seism. Soc. Am.*, **95**(3), 896-903.

Hileman, J. A., C. R. Allen & J. M. Nordquist, 1973. *Seismicity of the Southern California Region, 1 January 1932 to 31 December 1972*, Cal. Inst. Technology, Pasadena.

Helmstetter, A., Y. Y. Kagan & D. D. Jackson, 2005. Importance of small earthquakes for stress transfers and earthquake triggering, *J. geophys. Res.*, **110**(5), B05S08, doi:10.1029/2004JB003286, pp. 1-13.

Kagan, Y. Y., 1981a. Spatial distribution of earthquakes: The three-point moment function, *Geophys. J. Roy. astr. Soc.*, **67**, 697-717.

Kagan, Y. Y., 1981b. Spatial distribution of earthquakes: The four-point moment function, *Geophys. J. Roy. astr. Soc.*, **67**, 719-733.

Kagan, Y. Y., 1982. Stochastic model of earthquake fault geometry, *Geophys. J. Roy. astr. Soc.*, **71**, 659-691.

Kagan, Y. Y., 1991a. Fractal dimension of brittle fracture, *J. Nonlinear Sci.*, **1**, 1-16. http://moho.ess.ucla.edu/~kagan/1991_Nonlin_science.pdf

Kagan, Y. Y., 1991b. Seismic moment distribution, *Geophys. J. Int.*, **106**, 123-134.

Kagan, Y. Y., 2003. Accuracy of modern global earthquake catalogs, *Phys. Earth Planet. Inter.*, **135**(2-3), 173-209.

Kagan, Y. Y., 2004. Short-term properties of earthquake catalogs and models of earthquake source, *Bull. seism. Soc. Am.*, **94**(4), 1207-1228.

Kagan, Y. Y. & H. Houston, 2005. Relation between mainshock rupture process and Omori's law for aftershock moment release rate, *Geophys. J. Int.*, **163**(3), 1039-1048.

Kagan, Y. Y. & D. D. Jackson, 1991. Long-term earthquake clustering, *Geophys. J. Int.*, **104**, 117-133.

Kagan, Y. Y., D. D. Jackson & Y. F. Rong, 2006. A new catalog of southern California earthquakes, 1800-2005, *Seism. Res. Lett.*, **77**(1), 30-38, http://scec.ess.ucla.edu/~ykagan/calif_index.html

Kagan, Y. Y. & L. Knopoff, 1978. Statistical study of the occurrence of shallow earthquakes, *Geophys. J. Roy. astr. Soc.*, **55**, 67-86.

Kagan, Y. Y. & L. Knopoff, 1980. Spatial distribution of earthquakes: The two-point correlation function, *Geophys. J. Roy. astr. Soc.*, **62**, 303-320.

Kagan, Y. Y., and D. Vere-Jones, 1996. Problems in the modelling and statistical analysis of earthquakes, in: *Lecture Notes in Statistics*, **114**, C. C. Heyde *et al.* eds., New York, Springer, pp. 398-425.

Kendall, D. G., D. Barden, T. K. Carne & H. Le, 1999. *Shape and Shape Theory*, New York, Wiley, pp. 306.

Kendall, M. G. & Moran, P. A. P., 1963. *Geometrical Probabilities*, Hafner, N. Y., 125 pp.

King, G., 1983. The accommodation of large strains in the upper lithosphere of the Earth and other solids by self-similar fault systems: the geometrical origin of *b*-value, *Pure appl. Geophys.*, **121**, 761-815.

Libicki, E. & Y. Ben-Zion, 2005. Stochastic Branching Models of Fault Surfaces and Estimated Fractal Dimension, *Pure appl. Geophys.*, **162**(6-7), 1077-1111.

Mandelbrot, B. B., 1983. *The Fractal Geometry of Nature*, W. H. Freeman, San Francisco, Calif., 2nd edition, pp. 468.

Marsaglia, G., 1972. Choosing a point from the surface of a sphere, *Ann. Math. Stat.*, **43**, 645-646.

Matheron, G., 1971. *The Theory of Regionalized Variables and its Applications*, Cahiers du Centre de Morphologie Mathematique de Fontainebleau, No. 5., 211 pp.

McCaffrey, R., 1997. Statistical significance of the seismic coupling coefficient, *Bull. seism. Soc. Am.*, **87**, 1069-1073.

Molchan, G. & T. Kronrod, 2005. On the spatial scaling of seismicity rate, *Geophys. J. Int.*, **162**(3), 899-909, doi:10.1111/j.1365-246X.2005.02693.x

Nagel, W. & Weiss, V., 2005. Crack STIT tessellations: Characterization of stationary random tessellations stable with respect to iteration, *Adv. Appl. Probab.*, **37**(4), 859-883.

Nerenberg, M. A. H. & C. Essex, 1990. Correlation dimension and systematic geometric effects, *Phys. Rev.*, **A42**, 7065-7074.

Ogata, Y. & K. Katsura, 1991. Maximum likelihood estimates of the fractal dimension for random point patterns, *Biometrika*, **78**, 463-474.

Okabe, A., Boots, B., Sugihara, K. & Chiu, S., 2000. *Spatial Tessellations: Concepts and Applications of Voronoi Diagrams*, 2nd ed., Wiley, Chichester, 671 pp.

Pisarenko, D. V. & V. F. Pisarenko, 1995. Statistical estimation of the correlation dimension, *Physics Letters A*, **197**, 31-39.

Preliminary Determination of Epicenters, (PDE), Monthly Listings (1999). U.S. Dept. Interior/Geol. Survey, Nat. Earthquake Inform. Center, January, pp. 47.

Richards, P. G., F. Waldhauser, D. Schaff, and W. Y. Kim, 2006. The applicability of modern methods of earthquake location, *Pure Appl. Geophys.*, **163**(2-3), 351-372.

Richards-Dinger, K. B. & P. M. Shearer, 2000. Earthquake locations in southern California obtained using source-specific station terms, *J. geophys. Res.*, **105**(B5), 10939-10960.

Ripley, B. D., 1988. *Statistical Inference for Spatial Processes*, Cambridge, Cambridge University Press, 148 pp.

Schmittbuhl, J., F. Schmitt & C. Scholz, 1995. Scaling invariance of crack surfaces, *J. geophys. Res.*, **100**(4), 5953-5974.

Shearer, P., E. Hauksson & G. Q. Lin, 2005. Southern California hypocenter relocation with waveform cross-correlation, part 2: Results using source-specific station terms and cluster analysis, *Bull. seism. Soc. Am.*, **95**(3), 904-915.

Small, C. G., 1996. *The Statistical Theory of Shape*, New York, Springer, pp. 227.

Smith, L. A., 1988. Intrinsic limits on dimension calculations, *Physics Letters A*, **133**, 283-288.

Sornette, D. & V. Pisarenko, 2003. Fractal plate tectonics, *Geophys. Res. Lett.*, **30**(3), 1105, doi:10.1029/2002GL015043.

Stoyan, D. & H. Stoyan, 1994. *Fractals, Random Shapes, and Point Fields: Methods of Geometrical Statistics*, New York, Wiley, pp. 389.

Thio, H. K. & H. Kanamori, 1996. Source complexity of the 1994 Northridge earthquake and its relation to aftershock mechanisms, *Bull. seism. Soc. Am.*, **86**, S84-S92.

Vere-Jones, D., 1999. On the fractal dimensions of point patterns, *Adv. Appl. Probab.*, **31**, 643-663.

Vere-Jones, D., R. B. Davies, D. Harte, T. Mikosch & Q. Wang, 1997. Problems and examples in the estimation of fractal dimension from meteorological and earthquake data, Eds. T. Subba Rao, M.B. Priestley & O. Lessi, In: *Proc. Int. Conf. on Application of Time Series in Physics, Astronomy and Meteorology*, Chapman & Hall, London, pp. 359-375.

Weiss, J. & D. Marsan, 2003. Three-dimensional mapping of dislocation avalanches: clustering and space/time coupling, *Science*, **299**, 89-92.

Wiemer, S. & M. Wyss, 2000. Minimum magnitude of completeness in earthquake catalogs: examples from Alaska, the western United States, and Japan, *Bull. seism. Soc. Am.*, **90**, 859-869.

Wolfram, S., 1999. *The Mathematica Book*, 4th ed., Cambridge University Press, pp. 1470.

Wyss, M., C. G. Sammis, R. M. Nadeau & S. Wiemer, 2004. Fractal dimension and *b*-value on creeping and locked patches of the San Andreas fault near Parkfield, California, *Bull. seism. Soc. Am.*, **94**, 410-421.

Yan Y. Kagan, Department of Earth and Space Sciences, University of California, Los Angeles, California, 90095-1567, USA; (e-mail: ykagan@ucla.edu)

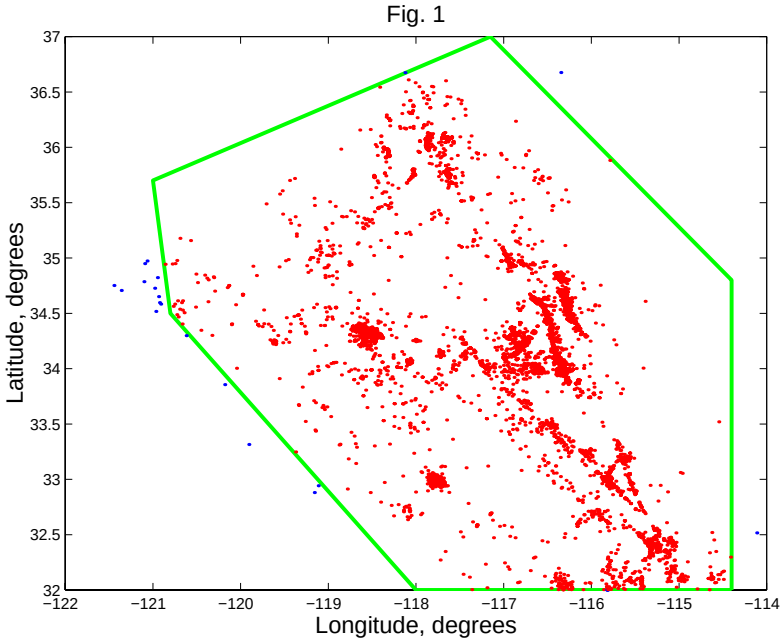

Figure 1. Epicenter distribution of earthquakes in southern California in the Hauksson & Shearer (2005) catalog. Time interval is 1984-2002, magnitude threshold $M_c = 3$. A 6-point box with the following coordinates is used: North latitude – 32.0°, 34.8°, 37.0°, 35.7°, 34.5°, 32.0°; West longitude – 114.4°, 114.4°, 117.15°, 121.0°, 120.8°, 118.0°. Earthquake distribution is considered to be reasonably homogeneous and complete in this box for the CalTech catalog (L. M. Jones, private communication, 2002). The area of the box is $S \approx 233,300$ km^2.

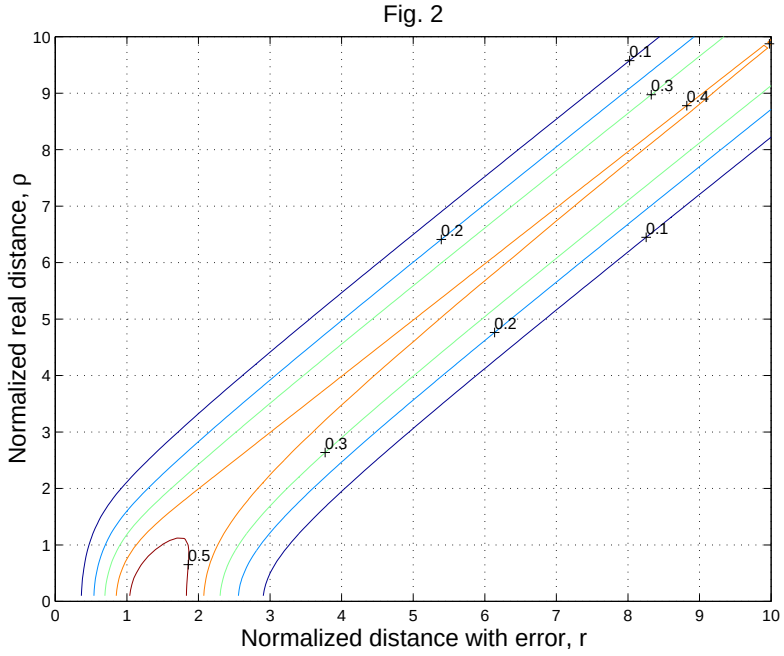

Figure 2. Density of non-central χ-distribution in 3-D.

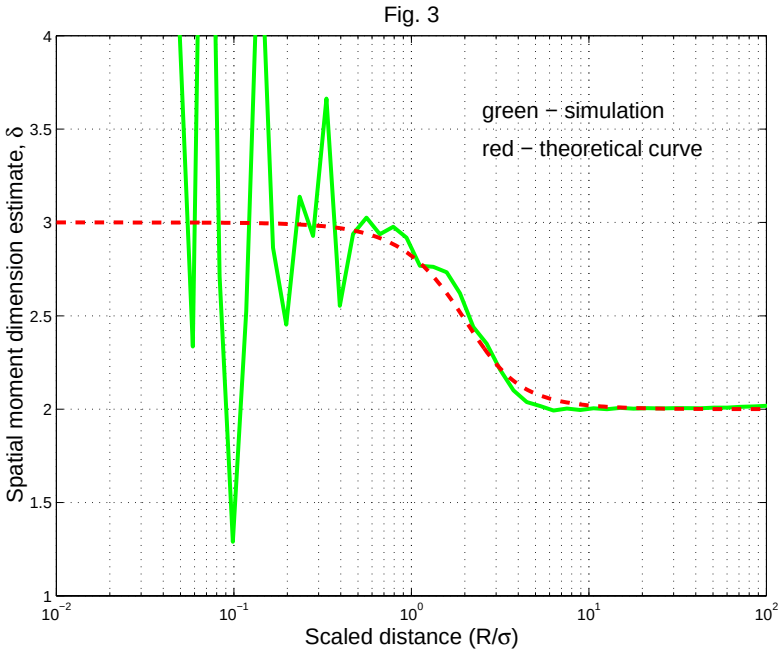

Figure 3. Dependence of the correlation dimension estimate $\hat{\delta}$ on distance scaled with the location error σ in 3-D. Solid line is simulation; dashed line shows $\hat{\delta}$ change according to (16).

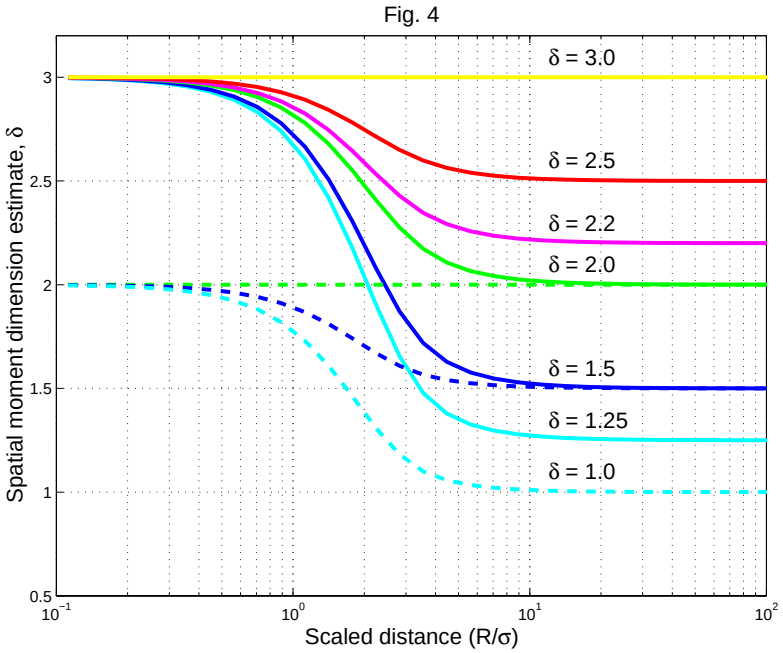

Figure 4. Dependence of the correlation dimension estimate $\hat{\delta}$ on distance scaled with the location error σ in 2-D and 3-D. Solid lines are for the 3-D distribution (hypocenters); dashed lines are for the 2-D distribution (epicenters). The initial fractal point dimension indicated as $\delta = 3$, etc.

Fig. 5

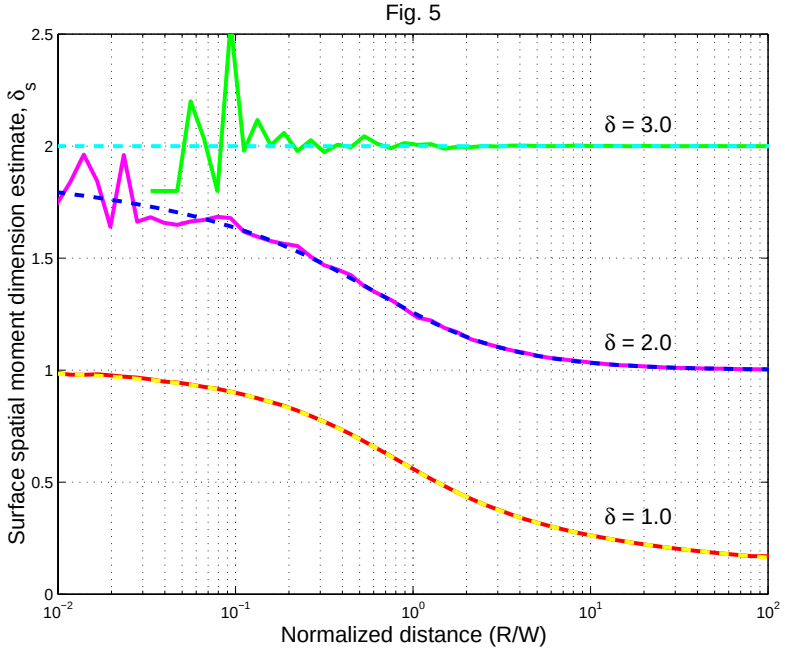

Figure 5. Dependence of the correlation dimension estimate $\hat{\delta}$ on scaled distance for epicenter distribution (grading effect). Three distributions in a layer of thickness W are simulated in 3-D: $\delta = 3$ or uniform Poisson distribution (upper two curves), with $\delta = 2$ (middle two curves), and with $\delta = 1$ (lower two curves). Dashed lines are theoretical curves (Eqs. 28–30); solid lines are simulation results.

Fig. 6

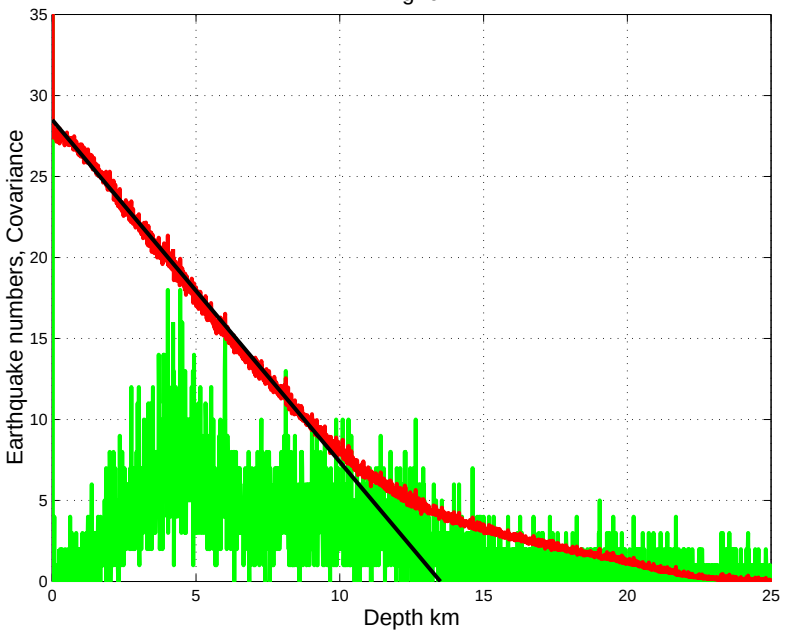

Figure 6. Depth dependence histogram (green lines) for the Hauksson & Shearer (2005) catalog ($M_c = 3$). Same events as in the box in Fig. 1. Depth correlation function (red line) and its approximation by linear function (black line), corresponding to a layer of thickness 13.5 km with uniform distribution of seismicity with depth.

Fig. 7

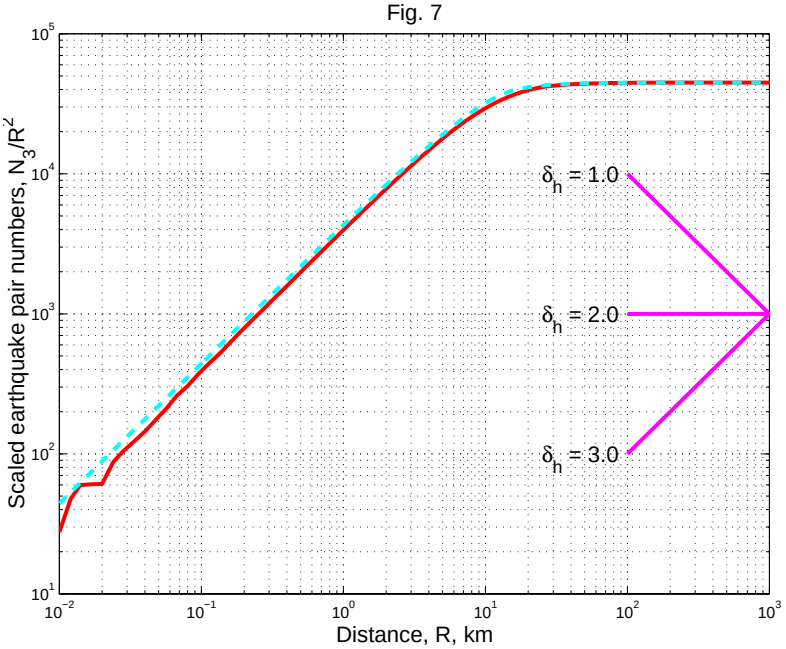

Figure 7. The expected number of event pairs in the southern California catalog. The theoretical curve (dashed line) is calculated for a layer with width W = 13.5 km having uniform seismicity distribution (39, 40). The solid line estimates the Hauksson & Shearer (2005) catalog (M_c = 3), corrected (43) by using the correlation function shown in Fig. 6. We normalize (divide) the earthquake pair number by R^2 so that the horizontal line would correspond to $\delta = 2$.

Fig. 8

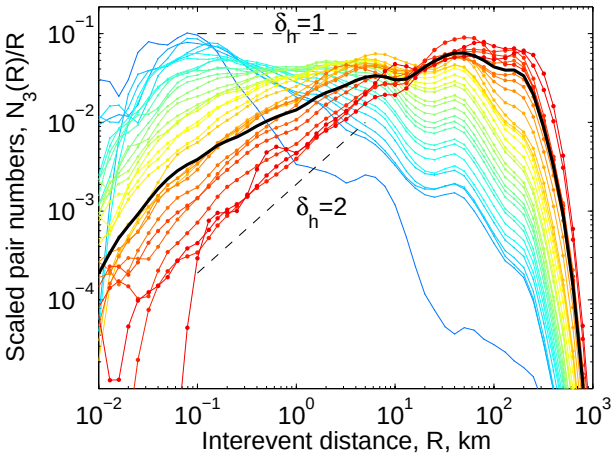

Figure 8. Distribution of distances between hypocenters $N_3(R,t)$ for the Hauksson & Shearer (2005) catalog, using only earthquake pairs with inter-event times in the range $[t,\ 1.25t]$. Time interval t increases between 1.4 minutes (blue curve) to 2500 days (red curve). We normalize (divide) the earthquake pair number by R so that the horizontal line would correspond to $\delta = 1$. The black line is the function $N_3(R)$ measured for all earthquake pairs; it has a fractal dimension $\hat{\delta} \approx 1.5$ for $0.1 \le R \le 5$ km.

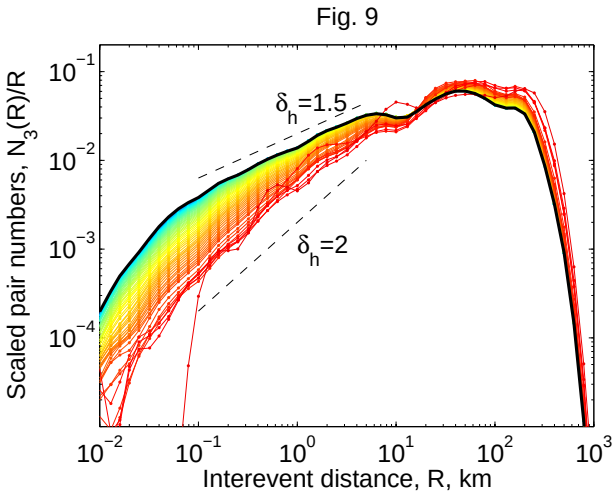

Figure 9. This diagram is similar to Figure 8 but for pairs with inter-event times larger than t.

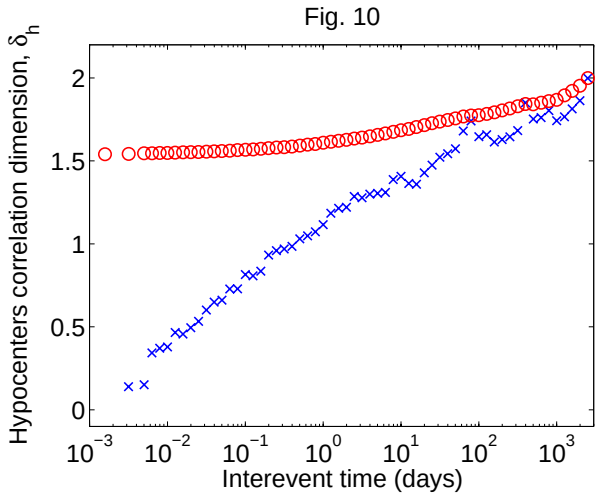

Figure 10. Fractal dimension of Figure 8 curves (crosses) and of Figure 9 curves (circles) as a function of time interval t. Distance interval is $0.1 \leq R \leq 5$ km.

Fig. 11

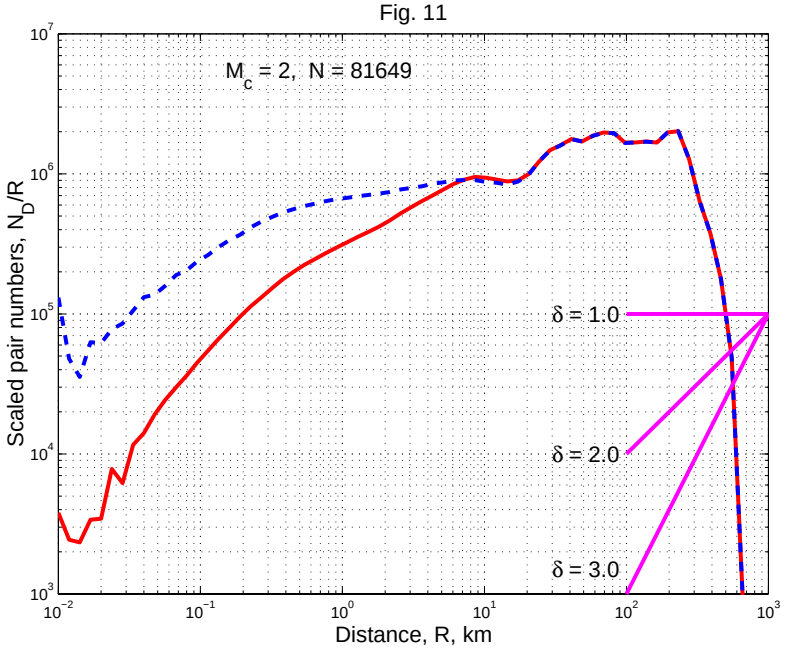

Figure 11. Hypocentral and epicentral spatial moment curves for the southern California waveform cross-correlation catalog 1984-2002 (Hauksson & Shearer 2005). Same events as in the box in Fig. 1. The magnitude threshold is $M_L \geq 2.0$, the total number of earthquakes $N = 81649$. The solid curve is for the hypocentral moment and the dashed for the epicentral.

Fig. 12

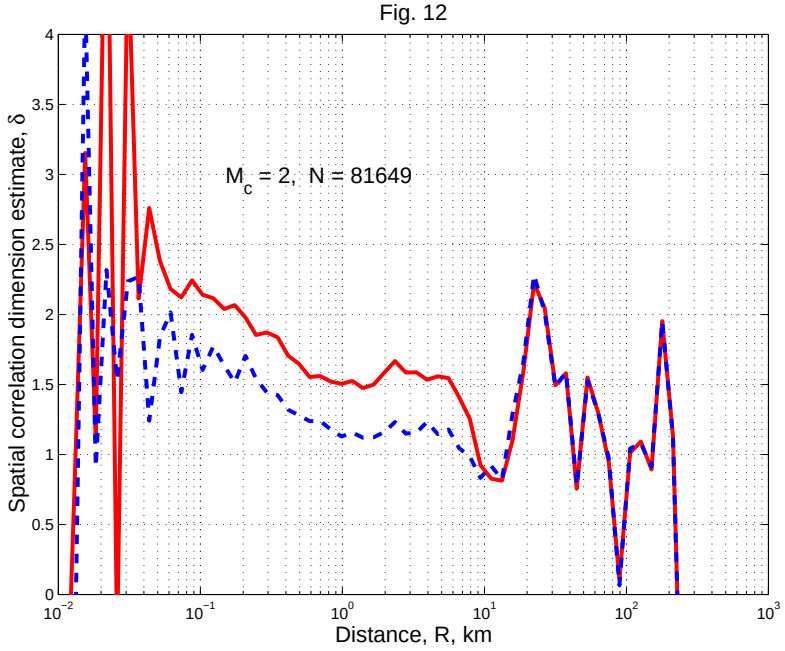

Figure 12. Correlation dimension estimate ($\hat{\delta}$) for the 1984-2002 Hauksson & Shearer (2005) catalog (Fig. 11). The solid curve is for the hypocentral moment and the dashed for the epicentral. The correlation dimension values are calculated as the distance scale is increased by a factor of $2^{1/4}$, starting with $R = 0.01$ km.

Fig. 13

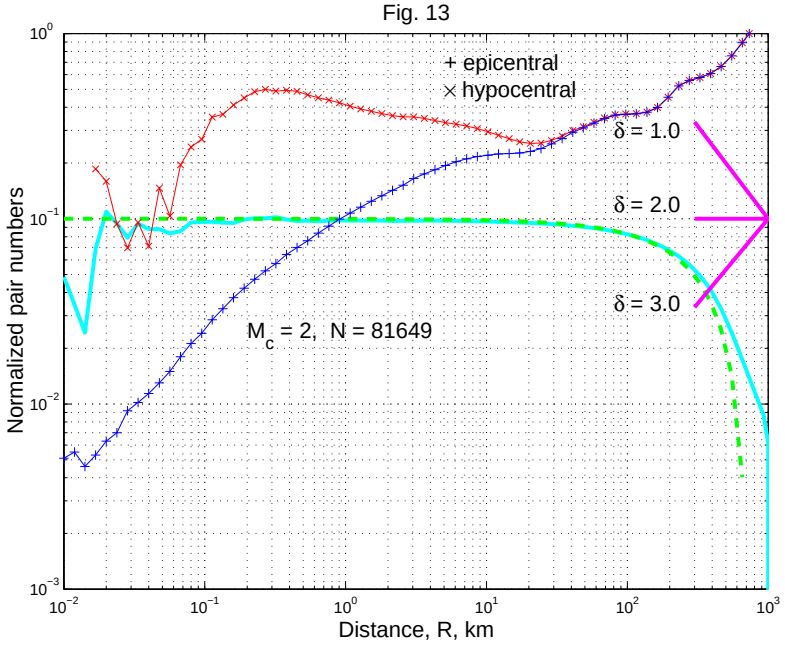

Figure 13. Hypocentral and epicentral spatial moment curves for the southern California waveform cross-correlation catalog 1984-2002, $M_L \geq 2.0$ (Hauksson & Shearer 2005). Same events as in the box in Fig. 1. The upper curve is for the hypocentral moment and the lower for the epicentral. Here we also plot two curves, demonstrating the boundary effects due to the limited spatial size of the catalog (see Section 4.4.1). The cyan solid curve is obtained by simulation for the box in Fig. 1. The green dashed line is calculated for a circle of radius 734.5 km (the maximum distance in the box). Magenta lines at the right show a slope of the curves corresponding to the integer values of the correlation dimension for the epicentral moment $\delta_s = \delta_h - 1$.

Fig. 14

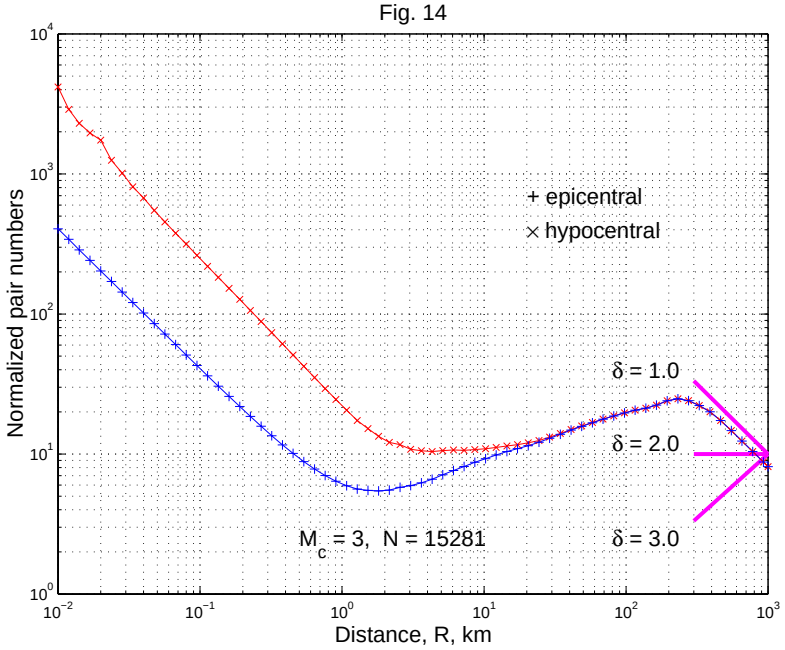

Figure 14. Hypocentral and epicentral spatial moment curves for the southern California (CalTech) catalog 1932-2001. Same box as in Fig. 1. The upper curve is for the hypocentral moment and the lower for the epicentral.

Fig. 15

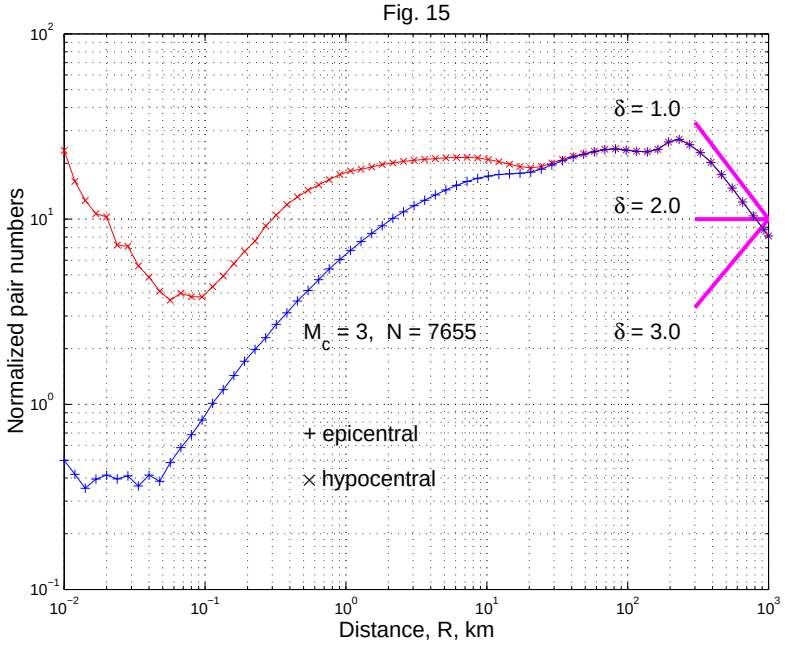

Figure 15. Hypocentral and epicentral spatial moment curves for the southern California (CalTech) catalog 1975-2001 ($M_L \geq 3.0$). Same box as in Fig. 1. The upper curve is for the hypocentral moment and the lower for the epicentral.

Fig. 16

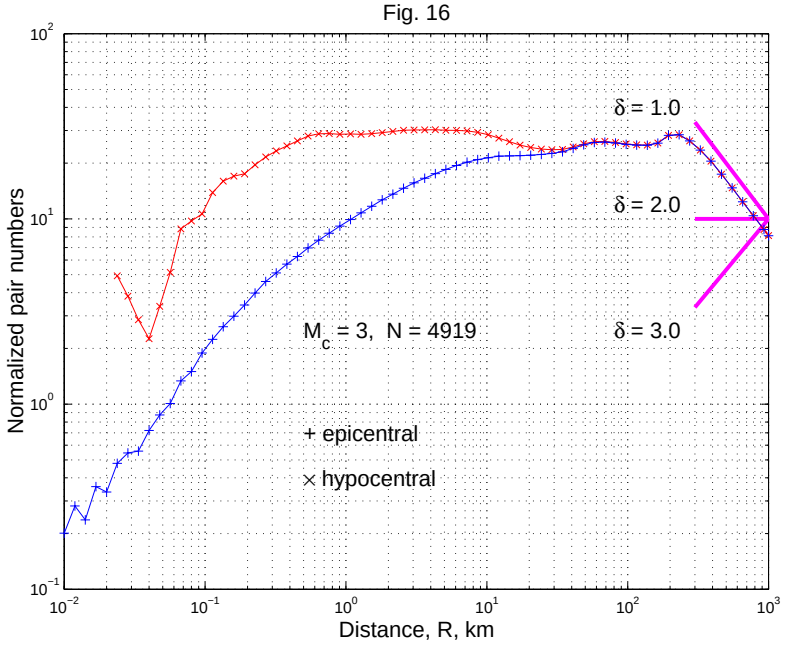

Figure 16. Hypocentral and epicentral spatial moment curves for the southern California relocated earthquakes catalog 1975-1997 (Richards-Dinger & Shearer 2000). Same box as in Fig. 1. Magnitude threshold is $M_L \geq 3.0$. The upper curve is for the hypocentral moment and the lower for the epicentral.

Fig. 17

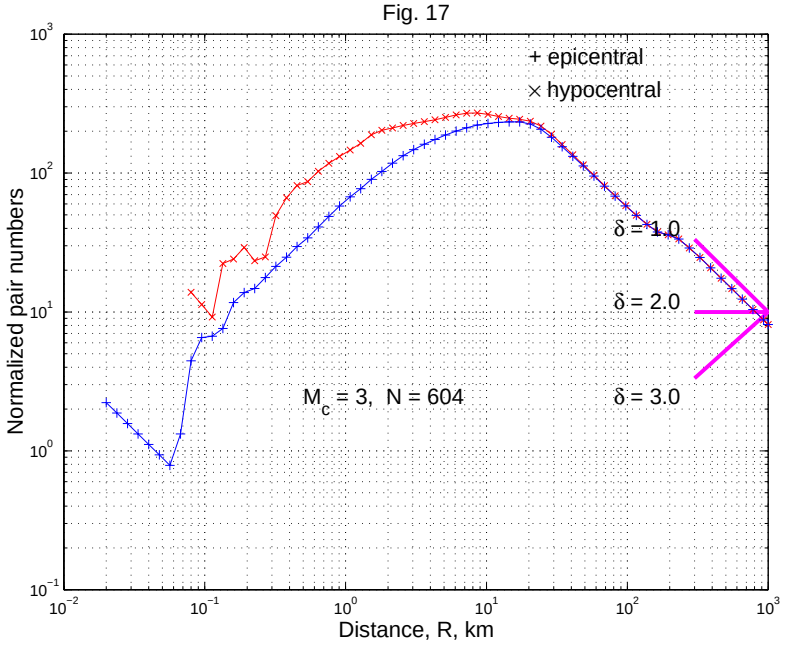

Figure 17. Hypocentral and epicentral spatial moment curves for the southern California (CalTech) catalog for 1994 ($M_L \geq 3.0$). Same box as in Fig. 1. The upper curve is for the hypocentral moment and the lower for the epicentral.

Fig. 18

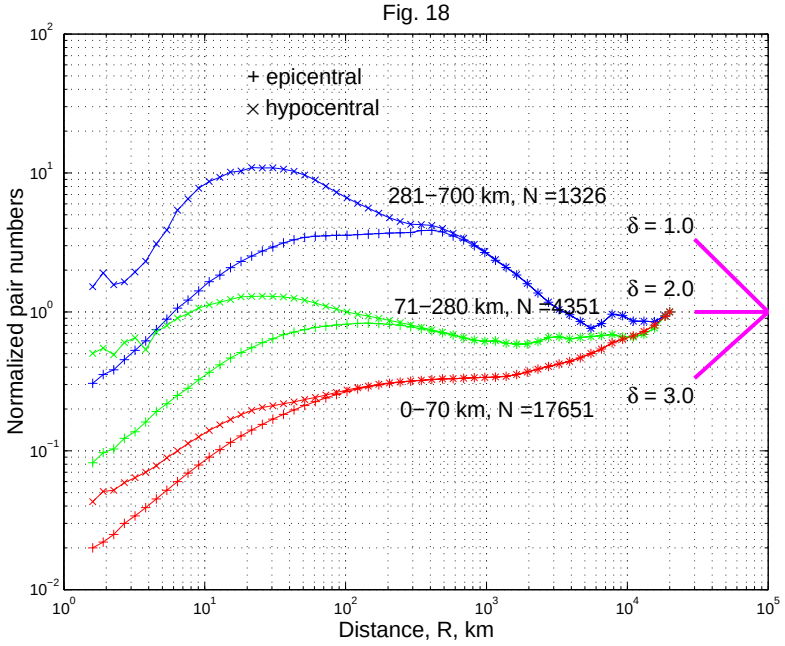

Figure 18. Hypocentral and epicentral spatial moment curves for various depth intervals. The PDE (1965-2003) catalog with $m_b \geq 5.3$ is used. In each of two curves, the upper one is for the hypocentral moment and the lower for the epicentral. Two upper curves are for the depth interval of 281-700 km; the middle curves are for the depth interval of 71-280 km; and the lower curves are for the depth interval of 0-70 km.